

Article

Environmental Assessment of Potentially Toxic Elements Using Pollution Indices and Data-Driven Modeling in Surface Sediment of the Littoral Shelf of the Mediterranean Sea Coast and Gamasa Estuary, Egypt

Magda M. Abou El-Safa ¹, Salah Elsayed ^{2,*}, Osama Elsherbiny ³, Adel H. Elmetwalli ⁴, Mohamed Gad ⁵, Farahat S. Moghanm ⁶, Ebrahim M. Eid ^{7,8}, Mostafa A. Taher ^{9,10}, Mohamed H. E. El-Morsy ^{11,12}, Hanan E. M. Osman ^{13,14} and Ali H. Saleh ¹

- ¹ Environmental Geology, Surveying of Natural Resources in Environmental Systems Department, Environmental Studies and Research Institute, University of Sadat City, Menoufia 32897, Egypt; magda.aboelsafa@esri.usc.edu.eg (M.M.A.E.-S.); ali.saleh@esri.usc.edu.eg (A.H.S.)
 - ² Agricultural Engineering, Evaluation of Natural Resources Department, Environmental Studies and Research Institute, University of Sadat City, Menoufia 32897, Egypt
 - ³ Agricultural Engineering Department, Faculty of Agriculture, Mansoura University, Mansoura 35516, Egypt; osama_algazeery@mans.edu.eg
 - ⁴ Department of Agricultural Engineering, Faculty of Agriculture, Tanta University, Tanta 31527, Egypt; adel.elmetwali@agr.tanta.edu.eg
 - ⁵ Hydrogeology, Evaluation of Natural Resources Department, Environmental Studies and Research Institute, University of Sadat City, Minufiya 32897, Egypt; mohamed.gad@esri.usc.edu.eg
 - ⁶ Soil and Water Department, Faculty of Agriculture, Kafrelsheikh University, Kafr El-Sheikh 33516, Egypt; fsaad@yahoo.ca
 - ⁷ Biology Department, College of Science, King Khalid University, Abha 61321, Saudi Arabia; ebrahim.eid@sci.kfs.edu.eg
 - ⁸ Botany Department, Faculty of Science, Kafrelsheikh University, Kafr El-Sheikh 33516, Egypt
 - ⁹ Biology Department, Faculty of Science and Arts, King Khalid University, Mohail Assir 61321, Saudi Arabia; mtaher@kku.edu.sa
 - ¹⁰ Botany Department, Faculty of Science, Aswan University, Aswan 81528, Egypt
 - ¹¹ Deanship of Scientific Research, Umm Al-Qura University, Makkah 24243, Saudi Arabia; mhmersy@uqu.edu.sa
 - ¹² Plant Ecology and Range Management Department, Desert Research Center, Cairo 11753, Egypt
 - ¹³ Biology Department, Faculty of Science, Umm-Al-Qura University, Makkah 24243, Saudi Arabia; heosman@uqu.edu.sa
 - ¹⁴ Botany and Microbiology Department, Faculty of Science, Al-Azhar University, Cairo 11651, Egypt
- * Correspondence: salah.emam@esri.usc.edu.eg



Citation: El-Safa, M.M.A.; Elsayed, S.; Elsherbiny, O.; Elmetwalli, A.H.; Gad, M.; Moghanm, F.S.; Eid, E.M.; Taher, M.A.; El-Morsy, M.H.E.; Osman, H.E.M.; et al. Environmental Assessment of Potentially Toxic Elements Using Pollution Indices and Data-Driven Modeling in Surface Sediment of the Littoral Shelf of the Mediterranean Sea Coast and Gamasa Estuary, Egypt. *J. Mar. Sci. Eng.* **2022**, *10*, 816. <https://doi.org/10.3390/jmse10060816>

Academic Editor: Gerardo Gold Bouchot

Received: 26 April 2022

Accepted: 9 June 2022

Published: 14 June 2022

Publisher's Note: MDPI stays neutral with regard to jurisdictional claims in published maps and institutional affiliations.



Copyright: © 2022 by the authors. Licensee MDPI, Basel, Switzerland. This article is an open access article distributed under the terms and conditions of the Creative Commons Attribution (CC BY) license (<https://creativecommons.org/licenses/by/4.0/>).

Abstract: Coastal environmental assessment techniques have evolved into one of the most important fields for the long-term development and management of coastal zones. So, the overall aim of the present investigation was to provide effective approaches for making informed decisions about the Gamasa coast sediment quality. Over a two-year investigation, sediment samples were meticulously collected from the Gamasa estuary and littoral shelf. The inductively coupled plasma mass spectra (ICP-MS) was used to the total concentrations of Al, Fe, Ti, Mg, Mn, Cu, P, V, Ba, Cr, Sr, Co, Ni, Zn, Pb, Zr, and Ce. Single elements environmental pollution indices including the geoaccumulation index (I_{geo}), contamination factor (CF), and enrichment factor (EF), as well as multi-elements pollution indices comprising the potential ecological risk index (RI), degree of contamination (Dc), and pollution load index (PLI) were used to assess the sediment and the various geo-environmental variables affecting the Mediterranean coastal system. Furthermore, the Dc, PLI, and RI were estimated using the random forest (RF) and Back-Propagation Neural Network (BPNN) depending on the selected elements. According to the Dc results, all the investigated sediment samples categories were considerably contaminated. Cr, Co, Ni, Cu, Zr, V, Zn, P, and Mn showed remarkable enrichment in sediment samples and were originated from anthropogenic sources based on the CF, EF, and I_{geo} data. Moreover, the RI findings revealed that all the samples tested pose a low ecologically risk. Meanwhile, based on PLI, 70% of the Gamasa estuary samples were polluted, while 93.75% of littoral

shelf sediment was unpolluted. The BPNNs -PCs-CD-17 model performed the best and demonstrated a better association between exceptional qualities and CD. With R^2 values of 1.00 for calibration (Cal.) and 1.00 for validation (Val.). The BPNNs -PCs-PLI-17 models performed the best in terms of measuring PLI with respective R^2 values of 1.00 and 0.98 for the Cal. and Val. datasets. The findings showed that the RF and BPNN models may be used to precisely quantify the pollution indices (Dc, PLI, and RI) in calibration (Cal.) and validation (Val.) datasets utilizing potentially toxic elements of surface sediment.

Keywords: contamination factor; RF; geoaccumulation index; enrichment factor; degree of contamination; BPNNs; potential ecological risk index

1. Introduction

Rapid economic and population growth has been accompanied by an increase in environmental contamination worldwide. Because of increased metal discharges from diverse sources, coastal and estuarine ecosystems are currently facing elevated metal pollution pressures. Potentially toxic elements (PTEs) contamination in the coastal environment has become one of the most critical environmental challenges and has received massive attention from researchers and governmental/nongovernmental associations due to its toxicity and persistence in the aquatic environment [1–5]. The mobility of potentially toxic elements in the aquatic environment is mostly governed by sediment compositions and human activities that may alter environmental parameters such as redox potential, pH, and biological activities [6]. Pollutants in the coastal environment mainly derive from continental sources entering the sea via rivers and their estuary [7]. PTEs in estuarine sediments can come from natural causes, including erosion, early diagenesis, and river transport, as well as anthropogenic contamination such as atmospheric deposition, wastewater discharge, aquaculture, agricultural activities, and industrial waste discharge [5,8–12].

Over time, estuary and coastal regions have been the focus of human settlement, resulting to the development of several large coastal cities around the world [13]. The coastal environment is dynamic and complicated due to the human activities, economy, ecology, and morphology that interact in it. The environmental assessment processes of coastal ecosystems have emerged as a significant field for the sustainable development and management of coastal zones. The purpose of maintaining the coastal resources is considered among the main pillars of continuous investment of coastal zones. Beach sediments are significant resources that must be reserved because their deterioration and pollution results in financial losses that affect the economic value of these beaches. Because of their abundance, toxicity, and potential ecological risk, assessment of heavy metals pollution in aquatic environment sediments using ecological risk assessment methodologies is crucial for the management of coastal zones [14,15].

The Nile Delta coast stretches about 280 km from the Mediterranean coast of Egypt. Several authors have been focused on the distribution of potential toxic metals in sediments along Egypt's Mediterranean coast and their environmental impact. For example, Okbah et al. [16] concluded that the Mediterranean coast recorded the highest concentration of metals in the Delta region, and the Egyptian Mediterranean coast sediments were enriched by Cr, Pb, and Ni; Soliman et al. [17]; stated that 15% and 35% of sediment samples exceeded the probable effect level in Cr and Ni respectively; El-Gamal and Saleh [18] mentioned that the Mediterranean delta coastal sediments were contaminated by Mo, Cd, and Ni particularly in El-Burullus and Rosetta sediments; Abdallah and Badr-EIDin [19] assessed the anthropogenic activities on sediment of Eastern Harbor at Alexandria City coast, and reported that about 86% of studied sediment were highly contaminated and the sediment was rich in Cd, Pb, As, and Hg; and Khaled et al. [20] evaluated the degree of contamination of potential toxic metals in sediments along Alexandria Coast and found that Cd and Pb were moderately enriched and contaminated the sediment. The Mediterranean

Sea coastal environment of Egypt is subjected to severe putting ashore of pollutants from numerous anthropogenic activities [18]. More than 50% of Egypt's population lives in the Nile Delta region [21]. Agriculture, fishing/aquaculture, industry, and recreation beaches are the main anthropogenic activities in the Nile Delta and its shores. About 70% of Egyptian industrial production and commercial activities are produced in the Nile Delta [22]. However, the status of the PTEs in the coastal environment has not been evaluated along the whole Mediterranean Sea coast of Egypt that extends over 1200 km, from El-Salloum west to Rafah east. As a result, evaluation techniques have become necessary to appraise the coastal sediment potential toxic elements concentrations, particularly in areas that have not been investigated previously.

Gamasa beach is regarded as one of the most important public resort beaches on the Nile Delta coast. It is situated on an accretionary and dynamic concave shoreline [23]. In the past decades, the Gamasa coast has been subjected to intensive development activities that threaten and impact the coastal environment. The direct possible environmental hazards resulting from such activities are sand encroachment and coastal erosion; indirect environmental hazards are contamination of coastal water and surface sediments by organic and inorganic pollutants. The Gamasa drain flows from south to north and pours into the Mediterranean Sea. Its end is crooked and protected by eastern and northern jetties. Data about trace elements in surface sediments of the Gamasa coastal zone and their ecological impacts and sources are very rare.

The prediction of pollution indices is a critical challenge in managing the ecosystem at a safe level. Various deterministic models have already been used in this area throughout the last few decades [24]. However, because real natural ecosystems are typically too sophisticated for these state-of-the-art models, their statistical efficiency is typically low. RF and ANNs may offer quick and robust techniques for developing models to estimate various pollution indices. ANNs and RF can generalize non-linear patterns within a specific dataset and solve complex issues [25]. These data-driven solutions can be utilized to solve severely nonlinear issues [26,27]. They have been effectively used to evaluate the accuracy of the water pollution constituent prediction [28].

There are a lack of data on the efficiency of ANNs and RF models combined with elements for estimating CD, PLI, and RI of surface sediment of estuary and coastal areas. Recently, a few attempts have been made to appraise the efficacy of ANNs, PLSR, and MLR approaches for quantifying pollution indices for sediments [27,29]. The results of studies conducted on the potential of using multivariate and ANNs models were promising and encouraged the use of such approaches in the field of precise estimating sediments quality directly from the potentially toxic elements data in Lake Qaroun under different conditions. The results showed the efficiency of the three tested models (ANNs, PLSR, and MLR) to predict PLI and RI revealing that the ANN is the best model to predict these parameters based on spectral reflectance indices as input parameters. For instance, the determination coefficient values of the ANN model of calibration datasets for predicting PLI and RI were 0.999, they were 0.897 and 0.853, respectively, for the validation dataset [27]. Saleh et al. [29] found that the calibration and validation models presented the best performance to predict the PLI, RI, and Dc based on the selected 21 elements: $R^2 = 0.948\text{--}0.991$ for PLSR, and $R^2 = 0.760\text{--}0.998$ for MLR. The proposed models can be used with different datasets, especially since we followed the leave-one-out validation (LOOV) approach with validation to measure the model behavior [27].

This research study aimed to provide effective tools for making informed decisions on surface sediment to ensure effective management, identify pollution sources, and provide a clear image of how sampling procedures might be modified.

In this regard, the specific objectives of the present study were to (i) evaluate the present circumstance of PTEs in surface sediments of the Gamasa estuary and littoral shelf; (ii) assess the ecological risks of PTEs by calculating (CF), (EF), (I_{geo}), (Dc), (PLI), and (RI); (iii) recognize the potential pollution provenance of PTEs using CA and PCA techniques; (iv) deduce the correctness of applying the BPNNs and RF models in quantifying the Dc,

PLI, and RI of bottom sediments; and finally, debate the possibility of using the RF and BPNs models as beneficial approaches for making informed-decisions concerning the ecological risk of anthropogenic metals in sediments.

2. Materials and Methods

2.1. Study Site Description

The Gamasa coast is characterized by a bar-built estuary created from a shallow bay conserved from the sea by a sand bar. The Gamasa shoreline extends for 28 km along the Nile Delta coast. The study area was located between latitudes of $31^{\circ}26'15''$ and $31^{\circ}27'00''$ N and longitudes of $31^{\circ}32'20''$ and $31^{\circ}34'33''$ E (Figure 1). The Gamasa littoral shelf is a significant portion of the Egyptian Mediterranean coast because it is immediately influenced by freshwater discharge from the Gamasa estuary, which is derived from the River Nile. It receives an assortment of effluents from domestic, industrial, and agricultural activities. The Gamasa drain receives about 13.1×10^6 m³/day of untreated sewage, agricultural, and industrial wastewater, such as Talkha fertilizer's factory wastewater [30].

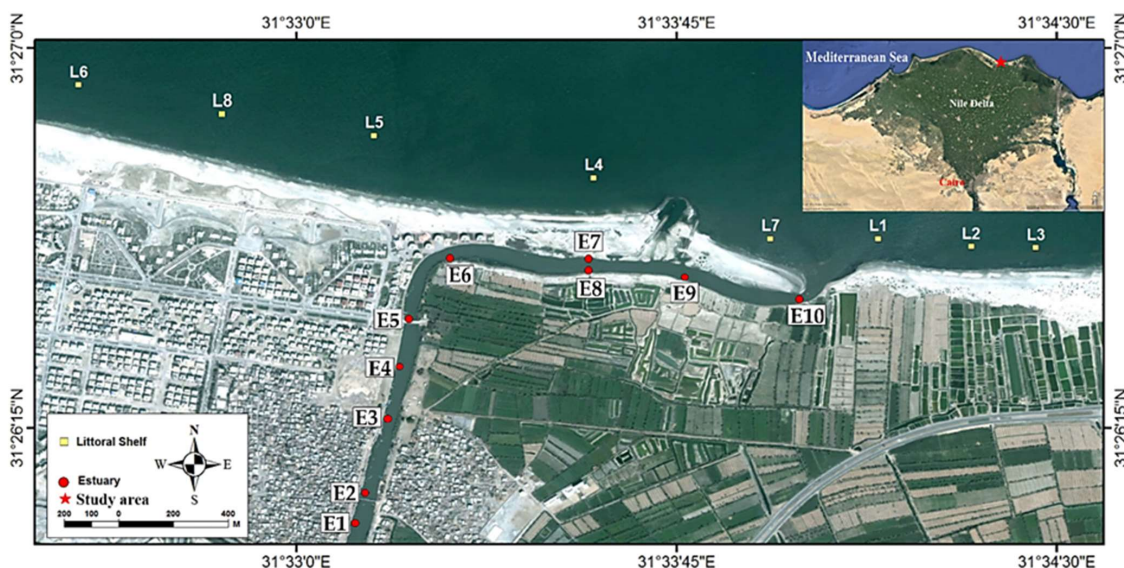


Figure 1. Location map of sampling points.

The current geomorphology of the Nile Delta's shore is the consequence of two opposing actions: delta advance and Mediterranean Sea attack via marine processes, followed by human activities as coastal protection constructions. Over the last century, the Nile Delta has experienced significant erosion and a massive retreat in shoreline, particularly at El-Burullus, the Rosetta, and Damietta headlands, and many conservation works have been performed around the Nile Delta coast to protect the eroding lands. The creation of the Nile Delta and its ancient branches is intimately tied to the geology of the beach sands alongside the Mediterranean shore [31].

2.2. Sample Gathering, Automated Inspection, and Quality Control

Over two years, sediment samples were gathered from the Gamasa estuary and littoral shelf of the Mediterranean Sea coast (Figure 1) using a stainless steel Peterson Grab sampler [32]. A fishing boat was used to reach different sampling points in the estuary and littoral shelf. A hand-held GPS (Garmin/eTrex Vista HCx/personal navigators) was used to identify the sampling location's position. For each location, three samples of sediment were taken. In order to avoid contamination from the metallic sampler, samples were gathered from the focus point of the grab sampler. The sampler was decontaminated between stations, carefully rinsed with site water and distilled water. Then it was suspended over a plastic container and washed from the top to down using a squirt bottle with 10% nitric

acid [33]. Before bringing the gathered materials to the laboratory, they were immediately sealed in polyethylene bags with identifying labels, which were then pre-washed before use. Subsamples for geochemical analysis were oven dried at 70 °C following natural drying at ambient temperature and filtered through a 2.0 mm sieve to achieve a consistent weight. Afterwards, samples were ground using an agate mechanical mill (Retsch RM200, Retsch, GmbH, Haan, Germany) and kept in glass containers while geochemical tests were performed. The metal concentrations were measured using ICP-MS (ICAP TQ ICP-MS Thermo Fisher Scientific Inc., Waltham, MA, USA). Using a SpeedWave microwave digestion apparatus, the sediment was transformed into a solution according to the US EPA 3052 method [34]. In a measuring flask, the digested solution was filtered, and deionized water was used to dilute it to a volume of 50 mL. Along with the investigated samples, blank samples (control) and one reference sample were digested. Quality control was carried out using replicated samples and the standard sediment reference components (GBW07333) supplied by China's 2nd Institute of Oceanography. All chemical reagents were analytical grade and ultrapure. Ultrapure water was used to make all the solutions. A Millipore apparatus system produced ultrapure water (Milli-Q) with 18.2 MΩ·cm resistivity. To avoid contamination, the test vessel and any used glass were properly cleaned and steeped in dilute nitric acid for at least 24 h before being drenched and rinsed with deionized water. The procedures were carried out in labs at the University of Sadat City that are accredited (ISO/IEC 17025/2017).

2.3. Pollution Assessment Indices

The environmental pollution assessment indices were determined to evaluate the potentially toxic elements contamination degree in the Gamasa estuary and littoral shelf surface sediments. The CF, EF, and I_{geo} approaches were applied to estimate a single element, and RI, PLI, and Dc were used to evaluate the combined hazard of several elements.

The contamination factor (CF) was determined according to [35] to quantify the contamination of sediments with trace metals. The contamination factor was classified according to the categories listed in Table 1.

The contamination degree (Dc) was suggested by [35] for applying in the processes of the sediment contamination total assessment. It is calculated by the equation found in Table 1; four levels of contamination are listed in Table 1, depending on the values of the contamination level.

The enrichment factor (EF) is a robust technique to differentiate between human and natural sources of trace elements in sediments [36,37]. It is usually used to assess the danger of heavy metal contamination in air aerosols, sediments, soil, and solid wastes, as well as to quantify the degree of fluctuation in their concentrations caused by human activity [38–40]. In order to determine the EF, we used the equation in Table 1. According to enrichment factors, seven distinct types of contamination may be distinguished (Table 1).

The geoaccumulation index (I_{geo}) proposed by Müller [41] is a useful tool to identify whether the sediment has been contaminated by anthropogenic heavy metals or not [42]. The Geoaccumulation index was calculated using the equation mentioned in Table 1. According to the geoaccumulation index results, the sediment contamination level may be classified to a scale varying from <1 to >5 to seven classes that were provided in Table 1.

The pollution load index (PLI) is great for comparing the overall pollution status at various sites (Table 1). For all elements at each sample, the PLI was calculated as the n th root of the CF multiplications [43,44]. The PLI of the Gamasa estuary and littoral shelf was calculated as the n th root of the PLI multiplications of the estuary and littoral shelf samples.

The Potential ecological risk index (RI) was applied to assess the ecological risk of heavy metals in sediments [35,45,46]. Four factors are considered: concentration, contaminant type, the toxicity level, and the sensitivity of the water body to metal contamination in sediments. Table 1 contains the formulae used to determine the RI. The toxic response factor for Mn, Cr, Co, Ni, Cu, Zn, and Pb are 1, 2, 5, 6, 5, 1, 5, respectively [35,47,48]. According to Håkanson [35], the RI is classified into four classes that are described in Table 1.

Table 1. The pollution indices equations and their classifications: potential ecological risk index (RI), degree of contamination (Dc), pollution load index (PLI), contamination factor (CF), enrichment factor (EF), and geoaccumulation index (I_{geo}).

Pollution Indices	Equation	Indices Criteria	Classes	Reference
CF	$CF = \frac{M_x}{M_b}$ <p>M_x: the potential toxic metal concentration in sediment samples. M_b: the concentration in the unpolluted “baseline” sediment (background value).</p>	≤ 1 $1 < CF \leq 3$ $3 < CF \leq 6$ $6 < CF$	Low CF Moderate CF Considerable CF Very high	[35]
Dc	$Dc = \sum_{i=1}^n CF$ <p>CF: the contamination factor of each analyzed element in the sample. <i>i</i>: the number of analyzed elements.</p>	< 8 $8 < Dc < 16$ $16 < Dc < 32$ $Dc > 32$	Low Dc Moderate Dc Considerable Dc Very high Dc	[35]
EF	$EF_x = \frac{(C_x/C_{Al})_{sample}}{(C_x/C_{Al})_{background}}$ <p>$(C_x/C_{Al})_{sample}$: the metal to Al ratio in the tested sample. $(C_x/C_{Al})_{background}$: the value of the metal to Al ratio in the natural background.</p>	< 1 1–3 3–5 5–10 10–25 25–50 > 50	No enrichment Minor enrichment Moderate enrichment Moderately severe enrichment Severe enrichment Very severe enrichment Extremely severe enrichment	[49]
I_{geo}	$I_{geo} = \log_2 \left(\frac{C_n}{1.5B_n} \right)$ <p>C_n: the measured concentration of heavy metal <i>n</i> in the sampled sediment. B_n: the geochemical background of the element that is adapted from the literature.</p>	$I_{geo} \leq 0$ $0 < I_{geo} \leq 1$ $1 < I_{geo} \leq 2$ $2 < I_{geo} \leq 3$ $3 < I_{geo} \leq 4$ $4 < I_{geo} \leq 5$ $5 < I_{geo}$	Unpolluted Unpolluted to Moderately polluted Moderately polluted Moderately to strongly polluted Strongly polluted Strongly to extremely polluted Extremely polluted	[41]
PLI	$PLI = (CF1 \times CF2 \times CF3 \times \dots \times CFn)^{1/n}$	$1 > PLI$ $1 < PLI$	Unpolluted Polluted	[44]
RI	$RI = \sum Er$ $Er = Tr \times CF$ <p>Er: the potential ecological risk factor of an individual element. Tr: the toxic response factor. CF: the contamination factor.</p>	$RI < 150$ $150 < RI < 300$ $300 < RI < 600$ $600 < RI$	Low ecological risk Moderate ecological risk Considerable ecological risk Very high ecological risk	[35]

2.4. Data Analyses

The data of potential toxic metals in the surface sediment samples were analyzed statistically using PAST v.4.07 (Natural History Museum, University of Oslo, Oslo, Norway). The Shapiro–Wilk test was performed to determine if the data of the current investigation were normally distributed or not. Metal content values in various sediment samples were processed using descriptive statistical parameters (maximum, minimum, and mean). The normality test results ($p < 0.05$) revealed that the data of the sediment deviated from the normal distribution. The Kruskal–Wallis test was run to determine whether element concentrations were equal between various sampling stations. To find relationships between the geochemical features of sediment samples we used the Pearson correlation coefficient. Furthermore, significance thresholds of 0.05 and 0.001 *p*-value were detected. Multivariate statistical techniques such as cluster analysis (CA) and principal component analysis (PCA) were also employed to assess their links and possible causes [50]. In terms of metal concentration, CA (Ward’s method) was used to examine the similarities and variations between varying sampling sites [51]. Commonly used statistical methods (e.g., Pearson’s correlation, CA, and PCA) are effective tools for identifying contamination sources which have been reported by several investigations in sediment contamination [12,29,52].

2.5. Random Forest

RF can be used to determine the link between a single dependent variable and a number of independent variables. It is built on the foundation of regression trees or

multiple classes. It separates a certain dataset into numerous nodes within a homogenous subset termed a regression tree (ntree), and then uses recursive fractioning to average the outputs of all trees. Each tree is stretched to its maximum size using a bootstrap sample from the training dataset without influencing the selection of the input variables at each node. In the regression phase of each tree, RF uses randomization by picking a random subset of variables (mtry) for estimating the split at each node [53]. The leave-one-out validation (LOOV) approach was used to enhance the model’s two parameters (mtry and ntree) and lower the root mean squared error of the validation (RMSEV). The ntree rating was evaluated between 1 and 25, while the mtry rating was examined with various feature counts. After the model was trained with optimal parameters, all features were classified, and the best features were chosen based on variable important statistics [54]. The outcomes were gathered for all iterations, and several options for the ideal feature interaction were assessed to determine the best one with the least RMSEV.

2.6. Back-Propagation Neural Network (BPNN)

The BPNN is one of the most popular artificial neural networks [55]. It is composed of three different layers: (a) the input layer includes the neural network’s fundamental data, (b) the hidden layer acts as an intermediary layer between the independent input layer and the dependent output layer, and (c) the output layer produces the outputs of the inputs that were provided. The artificial neural network (ANN) is a sort of machine learning procedure that employs numerous layers to derive high-level properties from primitive input. The network has two hidden layers, with the nodes number controlled by the accuracy of the regression. The “activation” nodes are represented by the hidden layers, which are commonly denoted by weight. The last layer depicts the resulted layer, which displays the expected value of the quantified parameter. Artificial neural networks, which are generalized mathematical models that include a group of neurons or nodes coupled by weighted connections, may be used to represent pattern recognition and prediction [56,57].

With at least 1000 iterations, the neural network was trained. On the training dataset, the validation procedure with the LOOV method was performed to define the number of neurons in the concealed layer. To efficiently construct the method, the parameter of restricted memory Broyden–Fletcher–Goldfarb–Shanno (lbfgs) was served as a weight optimizer [58]. Glorfeld et al. [59], developed a method to explore the most useful feature to increase the predictive power of the regression model and reduce the dimensionality of the data.

$$M = \frac{\sum_{j=1}^{n_H} \left[\left(|I|_{P_j} / \sum_{k=1}^{n_p} |I|_{P_{j,k}} \right) |O|_j \right]}{\sum_{i=1}^{n_p} \left(\sum_{j=1}^{n_H} \left[\left(|I|_{P_{i,j}} / \sum_{k=1}^{n_p} |I|_{P_{i,j,k}} \right) |O|_j \right] \right)} \tag{1}$$

where M is the important measure for the input variable, n_p is the number of input variables, n_H is the number of hidden layer nodes, $|I|_{P_j}$ is the absolute value of the hidden layer weight corresponding to the p th input variable and the j th hidden layer, and $|O|_j$ is the absolute value of the output layer weight corresponding to the j th hidden layer.

2.7. Model Evaluation

Statistical indicators such as determination coefficient (R^2) and root mean square error (RMSE) were employed to evaluate regression models as described by [60,61]. All parameters are explicated as follows: F_{act} is the actual value that was estimated from laboratory calculations, F_p is predicted or simulated value, F_{ave} is the average value, and N is the total number of data points.

Root mean square error:

$$RMSE = \sqrt{\frac{1}{N} \sum_{i=1}^N (F_{act} - F_p)^2} \tag{2}$$

Coefficient of determination:

$$R^2 = \frac{\sum(F_{act} - F_p)^2}{\sum(F_{act} - F_{ave})^2} \quad (3)$$

2.8. Analytical Dataset and Software

For training and validation, a total of 36 samples with 17 features were applied. The training dataset was divided based on the leave-one-out cross-validation (LOOCV) procedure for training, and validation. In each trial, LOOCV eliminates one sample for validation and utilizes the remaining data for training. This strategy can reduce over-fitting and offer a more accurate evaluation of the predictive power of a model [62,63]. The feature selection, model establishment, and data analysis were implemented using Python 3.7.3. The RF and BPNN modules from the Scikit-learn library version 0.20.2 were used for regression tasks. The software was run on a PC with Intel Core i7-3630QM, 2.4 GHz CPU, and 8 GB RAM.

3. Results and Discussion

3.1. Elements in Sediment

The statistical description of the potentially toxic elements contents, including the minimum value, maximum value, and mean, is presented in Table 2. The PTEs concentration averages at various sampling sites are presented in Tables S1 and S2 of the Supplementary Materials. Among the 17 elements studied, Al, Fe, and Mg concentrations were higher in sediment samples from the estuary and littoral shelf; while Pb, Co, and Cu concentrations were lower in the estuary and littoral sediment samples. The findings showed that depending on the sample site location, bottom sediments accumulated components from similar provenance and ways. Our findings are in agreement with the results documented by other investigators who tested metal contents in surface sediment samples from the Egyptian's Mediterranean coastal environment. The high percentage of Fe and low concentration of Co and Cu in the littoral sediment of the Egyptian Mediterranean shore were also reported by Soliman et al. [17]; El Baz and Khalil [64]; and Khaled et al. [20]. The average concentration of all elements did not change significantly between the two tested years, except for a substantial increase in the mean content of Cu, Pb, Zr, and Ce in estuary samples. Meanwhile, mean concentrations of Zn and Ba elements in estuary samples were falling in addition to Cr in littoral sediments. Estuary samples had the greatest contents of Mn, P, Cu, Cr, Zn, Ba, and Pb, which might be attributed to anthropogenic activities such as agricultural effluents and untreated wastewater discharged into the estuary. The estuary is a zone between the river and the marine that provides a variety of critical ecosystem activities and services [65]. Anthropogenic contaminants such as fertilizers and possibly toxic elements tend to act as receptors and sinks in estuarine zones [66–68]. Combining urban activities with agricultural chemicals can increase the percentage of harmful metals and metalloids in the estuary [68,69]. The Gamasa drain branching from the Damietta branch receives amounts of untreated sewage, agricultural, and industrial wastewater [30]. The elevated levels of Al and Fe in the sediments suggested that a terrigenous substance contaminated them spontaneously [67].

Generally, the present study's findings were similar to those of previous Mediterranean investigations made in Egypt and other countries as presented in Table 3, or even lower or higher in other circumstances. Manganese recorded average concentration in the present study (3700 and 2300 ppm) in the estuary and coastal shelf, higher than results recorded in other Mediterranean coastal sediments of Egypt and other countries. The lead element average concentration (5.0 ppm) was, in general, lower than their concentration in the sediments of the Mediterranean coast of Egypt and other states except for some coastal sediments of Spain (5.7 ppm). The fluctuation in PTEs concentrations can be due to point sources of contamination obtained at sampling stations, such as river mouths or excavated sediment from port locations [70,71].

Table 2. Statistical description of elements concentrations (ppm), except Al, Fe, Ti, Mn, P, and Mg in %.

Elements	First Year (n = 54)						Second Year (n = 54)						Across Two Years (n = 108)					
	Min	Estuary Max	Mean	Min	Littoral Max	Mean	Min	Estuary Max	Mean	Min	Littoral Max	Mean	Min	Estuary Max	Mean	Min	Littoral Max	Mean
Al	3.69	7.71	4.95	4.20	4.90	4.47	3.69	7.57	4.96	4.17	4.95	4.47	3.69	7.71	4.95	4.17	4.95	4.47
Fe	2.34	5.12	3.24	3.14	4.49	4.04	2.39	5.14	3.25	3.26	4.47	4.03	2.34	5.14	3.25	3.14	4.49	4.03
Ti	0.47	0.86	0.60	0.71	0.79	0.76	0.46	0.84	0.60	0.72	0.79	0.76	0.46	0.86	0.60	0.71	0.79	0.76
Mn	0.24	0.51	0.37	0.18	0.28	0.23	0.28	0.50	0.37	0.18	0.29	0.23	0.24	0.51	0.37	0.18	0.29	0.23
Mg	1.01	1.97	1.48	1.81	2.10	1.95	1.33	1.83	1.47	1.86	2.29	1.98	1.01	1.97	1.48	1.81	2.29	1.96
P	0.12	0.16	0.14	0.06	0.08	0.07	0.10	0.17	0.13	0.06	0.08	0.07	0.10	0.17	0.14	0.06	0.08	0.07
V	115	163	130	162	250	202	116	151	130	182	234	205	115	163	130	162	250	203
Cr	115	162	138	142	290	232	101	159	138	170	273	222	101	162	138	142	290	227
Co	13.0	27.0	20.7	18.0	24.0	21.8	11.0	35.0	21.3	17.0	26.0	21.5	11.0	35.0	21.0	17.0	26.0	21.6
Ni	22.0	38.0	29.3	28.0	39.0	33.0	22.0	35.0	29.4	30.0	36.0	33.4	22.0	38.0	29.3	28.0	39.0	33.2
Cu	19.0	33.0	27.4	11.0	16.0	12.8	20.0	34.0	28.5	8.00	15.0	11.9	19.0	34.0	28.0	8.00	16.0	12.3
Zn	97.0	132	113	36.0	59.0	46.6	75.0	129	107	31.0	65.0	46.1	75.0	132	110	31.0	65.0	46.4
Sr	191	263	223	242	294	269	184	270	223	241	300	270	184	270	223	241	300	269
Ba	266	501	399	202	301	253	217	520	395	189	293	252	217	520	397	189	301	252
Pb	5.00	30.0	16.3	2.00	6.00	4.88	6.0	30.0	17.0	3.00	6.00	5.13	5.00	30.0	16.7	2.00	6.00	5.00
Zr	149	258	185	240	383	319	139	274	192	221	389	321	139	274	189	221	389	320
Ce	17.0	42.0	28.6	23.0	72.0	52.6	16.0	47.0	29.0	31.0	75.0	52.6	16.0	47.0	28.8	23.0	75.0	52.6

Table 3. Comparison of potentially toxic element averages (ppm) in surface sediment of the current investigation with other studies in the Mediterranean Sea region.

Region	Country	Al	Fe	Ti	Mn	Mg	P	V	Cr	Co	Ni	Cu	Zn	Sr	Ba	Pb	Zr	Ce	Reference	
Estuary	Egypt	49,500	32,500	6000	3700	14,800	1400	130	138	21.0	29.3	28.0	110	223	397	16.7	189	28.8	Present study	
Littoral shelf		44,700	40,300	7600	2300	19,600	700	203	227	21.6	33.2	12.3	46.4	269	252	5.00	320	52.6		
Mediterranean coast		-	13,256	-	381.0	-	-	-	82.74	8.24	25.93	8.46	22.19	-	-	13.17	-	-		[17]
Alexandria		-	93,145	-	469.19	-	-	-	58.25	39.2	71.2	41.71	75.31	-	-	92.93	-	-		[72]
Abu-Qir Bay		9424	15,904	-	233.37	-	-	22.66	-	-	-	13.64	50.93	-	-	8.2	-	-		[73]
Eastern Harbor		2167	-	-	-	-	-	-	9.86	-	-	-	-	-	-	81.1	-	-		[19]
Mediterranean coast		-	13,256	-	381.0	-	-	-	82.74	8.24	25.93	8.46	22.19	-	-	13.17	-	-		[16]
Mediterranean coast		-	17,175	-	553.2	-	-	-	-	-	-	11.3	27.2	-	-	14.75	-	-		[64]
Rosetta coast	-	109,560	-	553	510	1539	375	0.18	69.8	481	24.6	183	-	-	384	-	-	[74]		
Rades-Hamam Lif Coast	Tunisia	-	-	-	-	-	-	-	30.14	-	22.71	24.37	72.78	-	-	35.78	-	-	[75]	
Gulf of Gabès		-	5827	-	85.67	-	-	25.24	31.97	2.4	8.21	7.05	44.20	-	-	8.31	-	-	[76]	
Tetouan coast	Morocco	33,800	39,700	-	362.86	-	-	-	128.39	23.24	50.28	14.88	84.26	-	-	41.11	-	-	[77]	
Algeciras Bay	Spain	-	28,129	-	534	-	-	36.0	112.0	11.0	65.0	17.0	73.0	-	-	24.0	-	-	[78]	
Mediterranean coastline		-	-	-	-	-	-	-	15.07	-	7.73	3.29	30.6	-	-	5.7	-	-	[71]	
Sabratha	Libya	-	2084	-	36.21	-	-	-	-	5.59	22.65	17.3	26.55	-	-	11.69	-	-	[79]	
Mediterranean coastline	Lebanon	-	-	-	247	-	-	58.2	49.5	3.36	27.2	-	128	-	-	98.26	-	-	[80]	

3.2. Pollution Assessment Indices

3.2.1. Contamination Factor (CF)

The CF proposed by [35] is the first step to understand the level of contamination and toward risk assessment of PTEs in surface sediments of the Gamasa estuary and littoral shelf. Table 4 presents the CF descriptive statistical data obtained from the investigated sediment samples. The contamination factors for Al, Mg, Ni, Sr, Ba, and Ce are low contamination levels ($CF < 1$), meaning that the Gamasa estuary and littoral shelf sediment samples are unpoluted by those elements. Moreover, there is no contamination by Fe in estuary samples and no contamination in littoral shelf sediments by Zn, Pb, P, and Cu. The estuary samples were moderately contaminated ($1 < CF \leq 3$) by Ti, P, V, Cr, Co, Cu, Zn, Pb, and Zr; and Fe, Ti, V, Cr, Co, and Zr were middlingly polluted in the shelf sediments samples. In contrast, the Mn had very high contamination ($6 < CF$) in estuary sediment samples and considerable pollution ($3 < CF \leq 6$) in shelf investigated samples.

Table 4. The statistical analysis of contamination variables (CF) in sediment samples.

Elements	First Year (n = 54)						Second Year (n = 54)						Across Two Years (n = 108)					
	Min	Estuary Max	Mean	Min	Littoral Max	Mean	Min	Estuary Max	Mean	Min	Littoral Max	Mean	Min	Estuary Max	Mean	Min	Littoral Max	Mean
Al	0.46	0.96	0.62	0.52	0.61	0.56	0.46	0.94	0.62	0.52	0.62	0.56	0.46	0.96	0.62	0.52	0.62	0.56
Fe	0.67	1.46	0.93	0.90	1.28	1.15	0.68	1.47	0.93	0.93	1.28	1.15	0.67	1.47	0.93	0.90	1.28	1.15
Ti	0.94	1.72	1.20	1.42	1.58	1.51	0.91	1.68	1.20	1.44	1.58	1.52	0.91	1.72	1.20	1.42	1.58	1.51
Mn	4.00	8.50	6.17	3.00	4.67	3.76	4.65	8.39	6.20	3.07	4.91	3.78	4.00	8.50	6.18	3.00	4.91	3.77
Mg	0.44	0.86	0.64	0.79	0.91	0.85	0.58	0.80	0.64	0.81	0.99	0.86	0.44	0.86	0.64	0.79	0.99	0.85
P	1.09	1.45	1.26	0.55	0.72	0.63	0.87	1.52	1.23	0.57	0.73	0.64	0.87	1.52	1.24	0.55	0.73	0.64
V	1.11	1.57	1.25	1.56	2.40	1.95	1.12	1.45	1.25	1.75	2.25	1.97	1.11	1.57	1.25	1.56	2.40	1.96
Cr	1.35	1.91	1.63	1.67	3.41	2.73	1.19	1.87	1.63	2.00	3.21	2.61	1.19	1.91	1.63	1.67	3.41	2.67
Co	0.76	1.59	1.22	1.06	1.41	1.28	0.65	2.06	1.26	1.00	1.53	1.27	0.65	2.06	1.24	1.00	1.53	1.27
Ni	0.44	0.76	0.59	0.56	0.78	0.66	0.44	0.70	0.59	0.60	0.72	0.67	0.44	0.76	0.59	0.56	0.78	0.66
Cu	0.76	1.32	1.10	0.44	0.64	0.51	0.80	1.36	1.14	0.32	0.60	0.48	0.76	1.36	1.12	0.32	0.64	0.49
Zn	1.37	1.86	1.60	0.51	0.83	0.66	1.06	1.82	1.50	0.44	0.92	0.65	1.06	1.86	1.55	0.44	0.92	0.65
Sr	0.51	0.70	0.60	0.65	0.78	0.72	0.49	0.72	0.59	0.64	0.80	0.72	0.49	0.72	0.59	0.64	0.80	0.72
Ba	0.53	1.00	0.80	0.40	0.60	0.51	0.43	1.04	0.79	0.38	0.59	0.51	0.43	1.04	0.79	0.38	0.60	0.51
Pb	0.31	1.88	1.02	0.13	0.38	0.31	0.38	1.88	1.06	0.19	0.38	0.32	0.31	1.88	1.04	0.13	0.38	0.31
Zr	0.90	1.56	1.12	1.45	2.32	1.94	0.84	1.66	1.17	1.34	2.36	1.94	0.84	1.66	1.14	1.34	2.36	1.94
Ce	0.24	0.60	0.41	0.33	1.03	0.75	0.23	0.67	0.41	0.44	1.07	0.75	0.23	0.67	0.41	0.33	1.07	0.75

3.2.2. Enrichment Factor (EF)

The sediment enrichment factor (EF) is a frequently used parameter for assessing the impact of anthropogenic activities in sediments by distinguishing between natural and human sources of a single element [80,81]. Accordingly, EF values less than one suggest that the element mostly came from natural processes or crustal materials, whereas EF values greater than one indicates that the sources are more likely to be anthropogenic [82]. When the enrichment factor is normalized against the tested element's background value, the anthropogenic contamination prognosis becomes better [83]. The common elements employed as normalized elements in the enrichment factor calculation are aluminum (Al), manganese (Mn), titanium (Ti), and iron (Fe) [84,85]. Al was used as a normalizing element in this investigation because of its low mobility [86]. Table 5 represents the descriptive statistical data of EF obtained from the Gamasa estuary and littoral shelf sediment samples. The mainstream PTEs in tested sediment samples showed a wide range, from no enrichment to severe enrichment. According to EF results, the sediment samples of the Gamasa estuary were not enriched ($EF < 1$) by Ce and had minor enrichment ($1 < EF < 3$) by Fe, Ti, Mg, P, V, Cr, Co, Ni, Cu, Zn, Sr, Ba, Pb, and Zr. However, there was severe enrichment ($10 < EF < 25$) by Mn. The shelf samples registered the following: no enrichment for Ba, Cu, and Pb; minor enrichment for Fe, Ti, Mg, P, Co, Ni, Zn, Sr, and Ce; moderate enrichment ($3 < EF < 5$) for V, Cr, and Zr; and moderately severe enrichment ($5 < EF < 10$) for Mn. The variation in enrichment suggests that anthropogenic sources such as industrial activity, sewage disposal, agricultural activity, and residential and urban wastes, rather than natural sources, contribute more to enrichment in the area under investigation [87]. Municipal wastewater

discharges, sewage sludge, and fossil fuel burning are the essential anthropogenic sources of environmental manganese [88,89].

Table 5. The statistical description of enrichment factor (EF) in studied sediment samples.

Elements	First Year (n = 54)						Second Year (n = 54)						Across Two Years (n = 108)					
	Estuary		Littoral		Estuary		Littoral		Estuary		Littoral		Estuary		Littoral			
	Min	Max	Mean	Min	Max	Mean	Min	Max	Mean	Min	Max	Mean	Min	Max	Mean	Min	Max	Mean
Al	1.00	1.00	1.00	1.00	1.00	1.00	1.00	1.00	1.00	1.00	1.00	1.00	1.00	1.00	1.00	1.00	1.00	1.00
Fe	1.06	1.87	1.49	1.63	2.43	2.08	1.05	1.78	1.50	1.72	2.46	2.08	1.05	1.87	1.50	1.63	2.46	2.08
Ti	1.50	2.54	2.01	2.53	3.02	2.72	1.57	2.63	2.00	2.48	3.04	2.73	1.50	2.63	2.00	2.48	3.04	2.73
Mn	4.52	18.0	11.1	5.46	8.30	6.77	4.94	17.8	11.2	5.66	8.18	6.79	4.52	18.0	11.2	5.46	8.30	6.78
Mg	0.70	1.32	1.09	1.36	1.75	1.53	0.80	1.39	1.10	1.39	1.90	1.55	0.70	1.39	1.10	1.36	1.90	1.54
P	1.52	2.60	2.15	0.99	1.37	1.14	1.34	2.69	2.10	1.02	1.24	1.14	1.34	2.69	2.13	0.99	1.37	1.14
V	1.50	2.62	2.12	2.73	4.60	3.51	1.54	2.73	2.13	3.03	4.34	3.55	1.50	2.73	2.13	2.73	4.60	3.53
Cr	1.48	4.08	2.90	2.93	6.44	4.94	1.54	4.08	2.88	3.40	6.13	4.72	1.48	4.08	2.89	2.93	6.44	4.83
Co	0.91	3.08	2.15	1.93	2.68	2.31	0.99	4.22	2.27	1.84	2.83	2.28	0.91	4.22	2.21	1.84	2.83	2.29
Ni	0.62	1.35	1.00	0.92	1.48	1.19	0.59	1.53	1.01	0.97	1.31	1.20	0.59	1.53	1.01	0.92	1.48	1.20
Cu	0.91	2.88	1.94	0.72	1.23	0.92	1.08	2.89	2.02	0.54	1.10	0.86	0.91	2.89	1.98	0.54	1.23	0.89
Zn	1.59	3.83	2.84	0.96	1.51	1.18	1.42	3.81	2.68	0.81	1.69	1.18	1.42	3.83	2.76	0.81	1.69	1.18
Sr	0.73	1.14	1.00	1.12	1.44	1.29	0.72	1.18	1.00	1.15	1.41	1.30	0.72	1.18	1.00	1.12	1.44	1.29
Ba	0.85	2.19	1.42	0.74	1.08	0.91	0.67	2.26	1.41	0.73	1.08	0.91	0.67	2.26	1.41	0.73	1.08	0.91
Pb	0.39	4.09	2.01	0.24	0.71	0.55	0.50	4.09	2.06	0.36	0.69	0.58	0.39	4.09	2.04	0.24	0.71	0.56
Zr	1.24	2.68	1.89	2.56	4.44	3.49	1.35	3.40	1.98	2.32	4.55	3.52	1.24	3.40	1.94	2.32	4.55	3.51
Ce	0.52	0.80	0.65	0.62	1.95	1.36	0.50	0.83	0.66	0.77	1.97	1.36	0.50	0.83	0.66	0.62	1.97	1.36

3.2.3. Geoaccumulation Index (I_{geo})

Geoaccumulation index (I_{geo}) descriptive statistical results of the Gamasa estuary and Mediterranean shelf sediment samples are detailed in Table 6. The I_{geo} negative value of PTEs, indicates that the investigated site is virtually unpolluted due to the gradual gathering of potentially toxic elements. The trend of investigated sediment samples has I_{geo} values ranging between unpolluted and moderately to strongly polluted. The sediment samples from the estuary and shelf were unpolluted ($I_{geo} < 0$) by Al, Fe, Mg, P, Co, Cu, Ni, Sr, Ba, Pb, and Ce. In contrast, those samples were moderately ($1 < I_{geo} < 2$) to strongly polluted ($2 < I_{geo} < 3$) by Mn. In addition, the estuary samples were unpolluted to moderately polluted ($0 < I_{geo} < 1$) by Zn and Cr, and the shelf samples by Ti, V, Cr, and Zr.

3.2.4. Multielement Pollution Indices (Dc, PLI, RI)

Table 7 shows the descriptive statistical results of Dc, PLI, and RI in the Gamasa estuary and littoral shelf surface sediment samples. According to the findings of Dc detailed in Table 8, all the investigated sediment samples obtained from the Gamasa estuary and coastal shelf were considerably contaminated by tested the elements. The PLI outcomes (Table 8) showed that 70% of the Gamasa estuary samples is polluted and 93.75% of littoral shelf sediment is unpolluted. Finally, the results of the prospective ecological risk index revealed that all tested samples were classified as low ecological risk ($RI < 150$). The RI results are compatible with those of Soliman et al. [17], who confirmed that the sediment of the Mediterranean coast at the Gamasa district is classified as a low ecological risk according to RI.

Table 6. The statistical description of geoaccumulation index (I_{geo}) in studied sediment samples.

Elements	First Year (n = 54)					Second Year (n = 54)					Across Two Years (n = 108)							
	Min	Estuary Max	Mean	Min	Littoral Max	Mean	Min	Estuary Max	Mean	Min	Littoral Max	Mean	Min	Estuary Max	Mean	Min	Littoral Max	Mean
Al	-1.71	-0.65	-1.33	-1.52	-1.30	-1.43	-1.71	-0.67	-1.33	-1.53	-1.28	-1.43	-1.71	-0.65	-1.33	-1.53	-1.28	-1.43
Fe	-1.17	-0.04	-0.77	-0.74	-0.23	-0.39	-1.14	-0.03	-0.76	-0.69	-0.23	-0.39	-1.17	-0.03	-0.76	-0.74	-0.23	-0.39
Ti	-0.67	0.20	-0.35	-0.08	0.07	0.01	-0.72	0.17	-0.35	-0.06	0.08	0.01	-0.72	0.20	-0.35	-0.08	0.08	0.01
Mn	1.42	2.50	2.00	1.00	1.64	1.31	1.63	2.48	2.01	1.03	1.71	1.32	1.42	2.50	2.00	1.00	1.71	1.31
Mg	-1.77	-0.81	-1.24	-0.93	-0.72	-0.83	-1.38	-0.91	-1.23	-0.89	-0.59	-0.80	-1.77	-0.81	-1.24	-0.93	-0.59	-0.82
P	-0.46	-0.04	-0.26	-1.46	-1.06	-1.25	-0.79	0.02	-0.31	-1.39	-1.03	-1.24	-0.79	0.02	-0.28	-1.46	-1.03	-1.25
V	-0.44	0.06	-0.28	0.05	0.68	0.36	-0.43	-0.05	-0.27	0.22	0.58	0.39	-0.44	0.06	-0.27	0.05	0.68	0.38
Cr	-0.15	0.35	0.11	0.16	1.19	0.84	-0.34	0.32	0.10	0.42	1.10	0.78	-0.34	0.35	0.10	0.16	1.19	0.81
Co	-0.97	0.08	-0.34	-0.50	-0.09	-0.24	-1.21	0.46	-0.35	-0.58	0.03	-0.26	-1.21	0.46	-0.35	-0.58	0.03	-0.25
Ni	-1.77	-0.98	-1.37	-1.42	-0.94	-1.19	-1.77	-1.10	-1.37	-1.32	-1.06	-1.17	-1.77	-0.98	-1.37	-1.42	-0.94	-1.18
Cu	-0.98	-0.18	-0.47	-1.77	-1.23	-1.57	-0.91	-0.14	-0.42	-2.23	-1.32	-1.69	-0.98	-0.14	-0.44	-2.23	-1.23	-1.63
Zn	-0.13	0.31	0.08	-1.56	-0.85	-1.21	-0.51	0.28	-0.02	-1.78	-0.71	-1.25	-0.51	0.31	0.03	-1.78	-0.71	-1.23
Sr	-1.56	-1.10	-1.35	-1.22	-0.94	-1.07	-1.61	-1.06	-1.35	-1.22	-0.91	-1.06	-1.61	-1.06	-1.35	-1.22	-0.91	-1.07
Ba	-1.50	-0.58	-0.94	-1.89	-1.32	-1.58	-1.79	-0.53	-0.98	-1.99	-1.36	-1.59	-1.79	-0.53	-0.96	-1.99	-1.32	-1.58
Pb	-2.26	0.32	-0.94	-3.58	-2.00	-2.36	-2.00	0.32	-0.76	-3.00	-2.00	-2.26	-2.26	0.32	-0.85	-3.58	-2.00	-2.31
Zr	-0.73	0.06	-0.44	-0.04	0.63	0.35	-0.83	0.15	-0.39	-0.16	0.65	0.35	-0.83	0.15	-0.42	-0.16	0.65	0.35
Ce	-2.63	-1.32	-1.96	-2.19	-0.54	-1.11	-2.71	-1.16	-1.95	-1.76	-0.49	-1.06	-2.71	-1.16	-1.95	-2.19	-0.49	-1.08

Table 7. The statistical description of the degree of contamination (Dc), pollution load index (PLI), and potential ecological risk index (RI) in studied sediment samples.

Indices	First Year (n = 54)					Second Year (n = 54)					Cross Two Year (n = 108)							
	Min	Estuary Max	Mean	Min	Littoral Max	Mean	Min	Estuary Max	Mean	Min	Littoral Max	Mean	Min	Estuary Max	Mean	Min	Littoral Max	Mean
Dc	17.4	25.4	22.1	17.8	22.5	20.5	18.4	26.0	22.2	18.3	22.1	20.4	17.4	26.0	22.2	17.8	22.5	20.4
PLI	0.83	1.15	1.01	0.86	1.02	0.95	0.86	1.16	1.01	0.88	0.99	0.94	0.83	1.16	1.01	0.86	1.02	0.94
RI	21.2	40.6	31.2	22.4	27.2	24.3	22.7	41.9	31.8	20.4	26.2	24.0	21.2	41.9	31.5	20.4	27.2	24.1

Table 8. Assessment of the studied sediments based on categories of contamination degree (Dc), potential ecological risk index (RI), and pollution load index (PLI).

Indices	Classes	Estuary Sediment Samples (%)			Littoral Sediment Samples (%)		
		1st Year	2nd Year	Across Two Years	1st Year	2nd Year	Across Two Years
Degree of Contamination (Dc)	Low	0	0	0	0	0	0
	Moderate Dc	0	0	0	0	0	0
	Considerable Dc	100% (30 samples)	100% (30 samples)	100% (60 samples)	100% (24 samples)	100% (24 samples)	100% (48 samples)
	Very high Dc	0	0	0	0	0	0
Pollution Load Index (PLI)	Unpolluted	30% (9 samples)	30% (9 samples)	30% (18 samples)	87.5% (21 samples)	100% (24 samples)	93.75% (45 samples)
	Polluted	70% (21 samples)	70% (21 samples)	70% (42 samples)	12.5% (3 samples)	0	6.25% (3 samples)
Ecological Risk Index (RI)	Low ecological risk	100% (30 samples)	100% (30 samples)	100% (60 samples)	100% (24 samples)	100% (24 samples)	100% (48 samples)
	Moderate ecological risk	0	0	0	0	0	0
	Considerable ecological risk	0	0	0	0	0	0
	Very high ecological risk	0	0	0	0	0	0

3.3. Correlation Matrix

Pearson’s correlation matrix was run to evaluate the rate of similarity and examine the inter-relationships among the elements under investigation [90]. Tables 9 and 10 show the Pearson’s correlation analysis findings for PTEs in the Gamasa estuary and littoral shelf sediment samples across the two-year investigation. The results of estuary samples (Table 9) reveal strong positive correlations between Fe, Ti, Mg, V, Sr, and Ce and Al ($r = 0.9, 0.82, 0.62, 0.8, 0.81, \text{ and } 0.94$, respectively); Ti, Mg, V, Ni, Sr, and Ce with Fe ($r = 0.83, 0.73, 0.63, 0.5, 0.91, \text{ and } 0.89$, respectively); and Co, Cr, Zn, Ba, and Pb with Mn ($r = 0.63, 0.51, 0.67, 0.5, \text{ and } 0.72$, respectively). In contrast a negative correlation was found between Mn, Cr, Zn, and Pb with Al ($r = -0.69, -0.69, -0.63, \text{ and } -0.83$, respectively); and Mn, Cr, Zn, and Pb with Fe ($r = -0.51, -0.71, -0.6, \text{ and } -0.73$, respectively). Other significant relationships between Cr and Co ($r = 0.63$), Cu ($r = 0.66$), Zn ($r = 0.84$), Ba ($r = 0.73$), Pb ($r = 0.9$), and Ce ($r = -0.81$) were also found. The littoral shelf results (Table 10) showed no strong correlations between the tested elements and Al, except with Cu and Ni ($r = -0.6 \text{ and } -0.5$, respectively). Moreover, significant correlation between selected elements were found: Fe with Ti, Mn, P, Co, Zn, Sr, and Ba ($r = 0.67, 0.59, 0.53, 0.53, -0.68, 0.63, \text{ and } -0.73$, respectively); Ti with Mg, Zn, Ba, and Pb ($r = 0.59, -0.62, -0.56, \text{ and } -0.54$, respectively); Mn with P, V, and Ba ($r = 0.83, 0.58, -0.76$, respectively); and V with Ba, Pb, Zr, and Ce ($r = -0.58, -0.67, 0.8, \text{ and } 0.6$, respectively). Remarkable significant correlations between the above-mentioned elements are thought to imply that they may have a typical accumulation manner or come from the same contamination source. Because of its high resilience to weathering and erosion, Al is among the well-protected elements. The obtained data of the correlation matrix revealed that some elements have a significant correlation with Al. Such metals may be created from natural sources, or they may be anthropogenic in origin and bind to clay minerals [91,92]. In addition, several metals have a strong relationship with Fe. In terms of the factors that control the distribution of PTEs, the findings suggest that clay minerals and (oxy) hydroxides of iron perform a vital role in the distribution of PTEs in the samples tested.

Table 9. Pearson’s correlation matrix of PTEs in surface sediments of estuary.

	Al	Fe	Ti	Mn	Mg	P	V	Cr	Co	Ni	Cu	Zn	Sr	Ba	Pb	Zr	Ce
Al	1.00																
Fe	0.90	1.00															
Ti	0.82	0.83	1.00														
Mn	-0.69	-0.51	-0.48	1.00													
Mg	0.62	0.73	0.77	-0.14	1.00												
P	0.47	0.16	0.43	-0.44	0.26	1.00											
V	0.80	0.63	0.78	-0.58	0.55	0.68	1.00										
Cr	-0.69	-0.74	-0.38	0.62	-0.25	0.00	-0.31	1.00									
Co	-0.36	-0.26	0.02	0.51	0.23	0.11	0.02	0.63	1.00								
Ni	0.29	0.50	0.38	0.14	0.68	-0.08	0.26	-0.21	0.26	1.00							
Cu	-0.40	-0.36	-0.04	0.38	0.19	0.23	0.08	0.66	0.75	0.26	1.00						
Zn	-0.63	-0.60	-0.32	0.67	0.00	0.04	-0.31	0.84	0.72	0.09	0.77	1.00					
Sr	0.81	0.91	0.62	-0.51	0.54	-0.02	0.46	-0.83	-0.40	0.27	-0.59	-0.73	1.00				
Ba	-0.33	-0.27	-0.01	0.50	0.21	0.07	-0.08	0.73	0.81	0.18	0.65	0.77	-0.44	1.00			
Pb	-0.83	-0.73	-0.50	0.72	-0.25	-0.29	-0.53	0.90	0.64	0.00	0.68	0.87	-0.82	0.72	1.00		
Zr	0.47	0.28	0.33	-0.26	0.16	0.32	0.33	-0.20	-0.05	-0.23	-0.31	-0.25	0.37	-0.15	-0.41	1.00	
Ce	0.94	0.89	0.73	-0.72	0.46	0.34	0.69	-0.81	-0.47	0.16	-0.50	-0.75	0.89	-0.48	-0.90	0.47	1.00

Table 10. Pearson’s correlation matrix of PTEs in surface sediments of littoral shelf.

	Al	Fe	Ti	Mn	Mg	P	V	Cr	Co	Ni	Cu	Zn	Sr	Ba	Pb	Zr	Ce
Al	1.00																
Fe	-0.04	1.00															
Ti	-0.19	0.67	1.00														
Mn	0.28	0.59	0.48	1.00													
Mg	-0.15	0.27	0.59	0.08	1.00												
P	0.39	0.53	0.38	0.83	0.11	1.00											
V	-0.18	0.09	0.10	0.58	-0.03	0.56	1.00										
Cr	-0.36	0.23	0.24	0.43	0.12	0.16	0.36	1.00									
Co	-0.07	0.53	0.15	0.17	0.15	-0.05	-0.34	0.24	1.00								
Ni	-0.50	0.04	-0.27	-0.43	-0.16	-0.48	-0.12	-0.04	0.26	1.00							
Cu	-0.60	-0.33	0.04	-0.23	0.08	-0.42	0.18	-0.04	-0.28	0.11	1.00						
Zn	-0.20	-0.68	-0.62	-0.22	-0.73	-0.31	0.25	0.03	-0.40	0.10	0.41	1.00					
Sr	0.13	0.63	0.39	-0.02	0.38	0.12	-0.41	-0.29	0.35	0.24	-0.40	-0.80	1.00				
Ba	-0.01	-0.73	-0.56	-0.76	-0.03	-0.69	-0.58	-0.08	-0.04	0.11	0.00	0.25	-0.24	1.00			
Pb	0.18	-0.34	-0.54	-0.45	-0.27	-0.58	-0.67	0.03	0.34	0.18	-0.24	0.17	-0.09	0.71	1.00		
Zr	-0.31	-0.24	-0.21	0.33	-0.45	0.21	0.80	0.32	-0.29	-0.01	0.37	0.74	-0.75	-0.29	-0.35	1.00	
Ce	0.01	-0.42	-0.49	0.21	-0.55	0.14	0.60	0.17	-0.19	0.05	0.09	0.73	-0.73	-0.04	-0.03	0.84	1.00

3.4. Multivariate Statistical Analysis

3.4.1. Cluster Analysis

A single correlation study is insufficient to understand the origins of elements. As a result, CA and PCA have become popular methods for detecting element sources and their properties in sediment [93,94]. Figure 2 depicts the dendrogram extracted from the cluster analysis of elements in the Gamasa estuary and littoral shelf samples. The CA outcomes for various investigated elements in estuary samples (Figure 2A) contain four main clustering groups. The elements of Al and Fe forms the first group (cluster I), and the second group (cluster II) is composed of Mg. The third group (cluster III) consists of Ti and Mn. The fourth group (cluster IV) is subdivided into three sub-clusters; one group contains P; another group is composed of Co, Pb, Ni, Cu, and Ce; while the last one contains Zn, V, Cr, Sr, Zr, and Ba. In contrast, the littoral shelf cluster analysis (Figure 2B) indicates three main clusters: (cluster I) Mg, Al, and Fe; (cluster II) Ti; (cluster III) and divided into three subgroups. The three subgroups are composed of the following (1) Mn; (2) Zr, Ce, Cu, Pb, Co, and Ni; and (3) Zr, V, Cr, Sr, Ba, and P. Despite the similarity in the presence of harmful elements and fluctuations in their concentrations, as shown by the dendrogram, the Euclidean distances between these two groups are vastly different. The smaller distance indicates that they are closely connected.

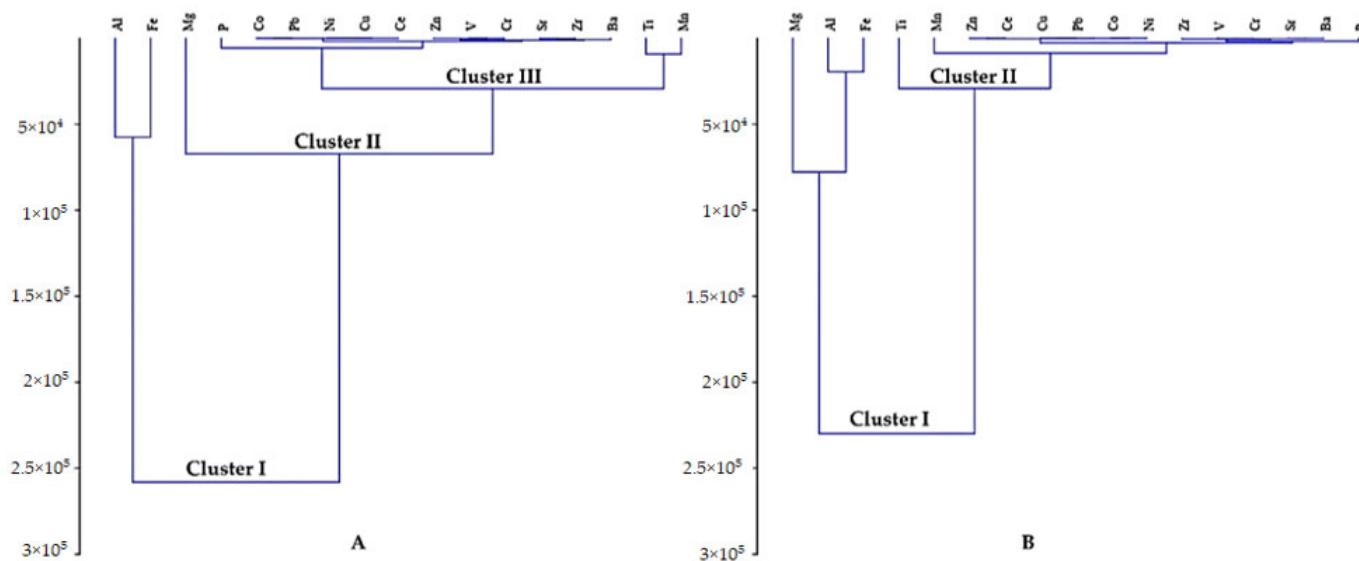


Figure 2. A dendrogram presented the elements clusters in sediment samples of (A) estuary and (B) littoral shelf.

3.4.2. Principal Component Analysis

PCA analysis was performed to find similarities between observed parameters (PTEs) and pinpoint the source of their origin (Figure 3). The PCA of estuary samples demonstrated two significant elements explaining in total 99.195% of the variance. The first PC1 described 94.26% of the whole variance controlled by notable Al loading and Fe (loading 0.795 and 0.598, respectively), especially from samples No. E6, E8, E9, E10, E16, E18, E19, and E20. The PC2 explained 4.935% of the total variance and composed mainly Mg, Mn, and Ti (loading 0.172, 0.092, and 0.026, respectively). The shelf samples displayed the following three principal components: (1) PC1 elucidated 75.151% of total variance and composed mainly Fe, Mg, Mn, and Ti (loading 0.996, 0.068, 0.042, and 0.035, respectively); (2) PC2 explained 20.702% of total variance; (3) and PC3 elucidated 3.837% variance. The PCA results revealed an elevated loading of Al and Fe in the basic components, as well as significant increasing correlations with Al and Fe in other investigated elements in the same components, meaning that these metals occur naturally in sediment or are derived from anthropogenic sources and have a distribution pattern governed by clay minerals and iron oxides. All the above-described findings suggest that the metals in investigated sediment samples may come from a variety of sources (natural and anthropogenic). The findings suggest that anthropogenic activity is the primary source of the potential environmental hazardous elements Cu, Ni, Co, Mn, V, Zn, P, and Cr found in surface sediment samples from the Gamasa estuary and coastal shelf.

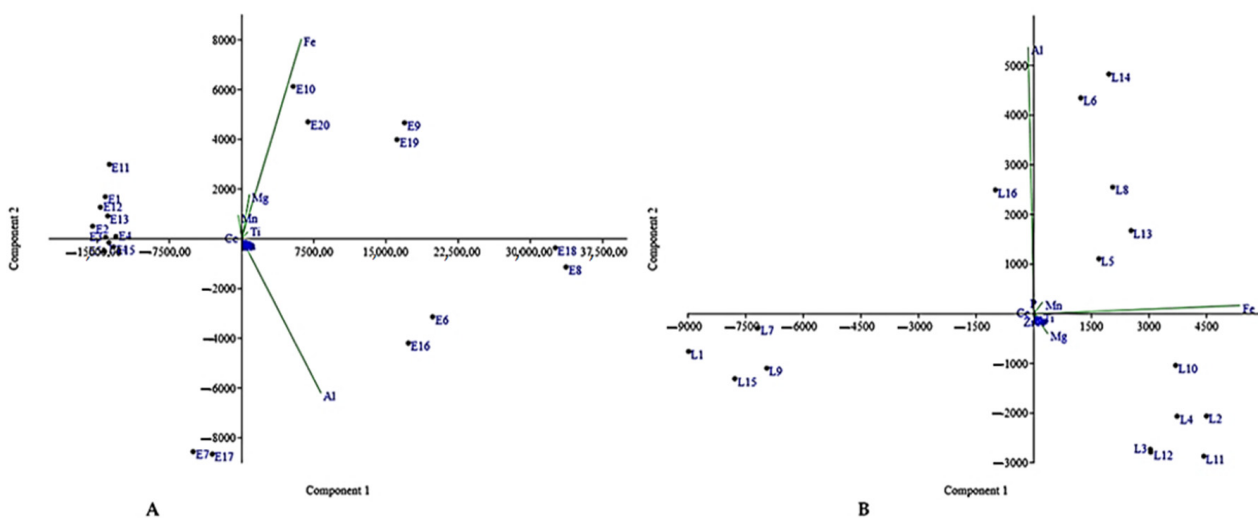


Figure 3. Principal component analysis for elements of (A) estuary and (B) littoral shelf sediment samples.

3.5. Performance of Random Forest and Artificial Neural Networks Based on Several Elements to Assess Pollution Indices

The RF and BPNN models were used in this study to forecast pollution indices depending on a range of elements as seen Tables 11 and 12. The traditional mathematical approaches discussed in this study can be utilized to provide approximate CD, PLI, and RI forecasts for sediment samples [35,44]. The use of RF and BPNN as an alternate approach for predicting these indices was assessed in the present research since it is rapid, simple, and does not necessarily require multiple steps to calculate CD, PLI, and RI. ANNs have lately shown outstanding performance as a regression approach, particularly when applied for function determination and pattern recognition. In comparison to traditional approaches, ANN can tolerate and interpret incomplete datasets, produce conclusions, and is less vulnerable to outliers [25,95].

Table 11. Results of validation models of random forest of the association between observed and predicted of degree of contamination (CD), pollution load index (PLI), and potential ecological risk index (RI) in two years.

Variable	Parameters	Sort by Lowest to Highest	Calibration		Validation	
			R ²	RMSE	R ²	RMSE
CD	ntree = 2, mtry = 10	Pb, Ni, Ce, Cu, Cr, Mg, P, Ti, Fe, V, Ba, Co, Sr, Al, Zr, Mn, Zn	0.92 ***	0.623	0.85 ***	0.655
PLI	ntree = 5, mtry = 8	Ti, V, Cu, Mg, Sr, Fe, Ni, Co, P, Mn, Cr, Zr, Ce, Pb, Al, Zn, Ba	0.95 ***	0.017	0.80 ***	0.026
RI	ntree = 30, mtry = 5	V, P, Mg, Ti, Ni, Cr, Co, Fe, Cu, Ba, Zr, Sr, Mn, Al, Ce, Zn, Pb	0.99 ***	0.714	0.90 ***	1.464

*** Statistically significant at $p \leq 0.001$.

Table 12. Outcomes of calibration and validation models of ANN of the association between observed and predicted for potential ecological risk index (RI), contamination degree (CD), and pollution load index (PLI) in the two-year investigation.

Variable	Parameters	Sort by Lowest to Highest	Calibration		Validation	
			R ²	RMSE	R ²	RMSE
CD	(18,22) identity	Zr, Ba, Sr, Mg, Ti, Cu, Co, Cr, Pb, Al, Ce, V, Fe, Zn, P, Ni, Mn	1.00 ***	0.0003	1.00 ***	0.0004
PLI	(22,12) logistic	Cr, Fe, Ba, V, Ti, P, Mn, Cu, Zr Ni, Mg, Sr, Co, Ce, Al, Zn, Pb	1.00 ***	0.0047	0.98 ***	0.0078
RI	(22,12) identity	Ba, Fe, P, Zn, Ti, Sr, Cu, Ce, Mn, Ni, Zr, Mg, V, Al, Cr, Co, Pb	1.00 ***	0.0001	1.00 ***	0.0004

*** Statistically significant at $p \leq 0.001$.

The best proposed components (PCs), optimal parameters, and RF model outputs for RMSE and R2 are shown in Table 9 for the calibration (Cal.) and validation (Val.) datasets. Based on R2 (Table 11) and slope (Figure 4), the RF model produced a more accurate evaluation of CD, PLI, and RI in both models of the Cal. and Val. The outcomes of advanced models were optimized by including the best characteristics. The RF-PCs-CD-17 model performed better in predicting CD and was constructed using two (ntree: number of trees) and ten (ntree: number of trees); R2 and RMSE increased to 0.85 and 0.655, respectively, using this model. For predicting PLI, the RF-PCs-PLI-17 model obtained a high expectation at 5 ntree and 8 mtry; the performance increased to 0.80 and 0.026 for R2 and RMSE, respectively. To estimate RI, the RF-PCs-RI-17 model was built using 30 ntree and 5 ntry; the R2 climbed to 0.90, while the RMSE reduced to 1.464. The suggested RF models acquired great performance by tuning hyperparameters and choosing the optimal indices. High performance was attained by the suggested RF models by following a set of methods, which included tuning hyperparameters and choosing the optimum indices [96].

Figure 5 illustrates the neural network topologies developed after collecting senior sediment characteristics. The figure depicted the optimal neural network topology based on the versions selected. Each network’s architecture contains basic information about the learned synaptic weights, the number of unseen neuron layers, the convergence stages, and the total errors. The network architecture is created by combining a number of input variables with a number of concealed neuron layers. For example, the model ANN-PCs-CD-17 has hidden neuron layers (18,22), the model ANN-PCs-PLI-17 was required (22,12), and the model ANN-PCs-RI-17 was selected (22,12). In Figure 6, advanced models of ANN-PCs-CD-17, ANN-PCs-PLI-17, and ANN-PCs-RI-17 are shown. To achieve a reduced error function, the training method required 554, 392, and 534 steps, respectively. The procedure had a total error of around 6×10^{-6} , 1.2×10^{-5} , and 8×10^{-6} , respectively. According to

Thawornwong and Enke [97], the network was trained using the back-propagation method with early halting to keep over-fitting at a minimum.

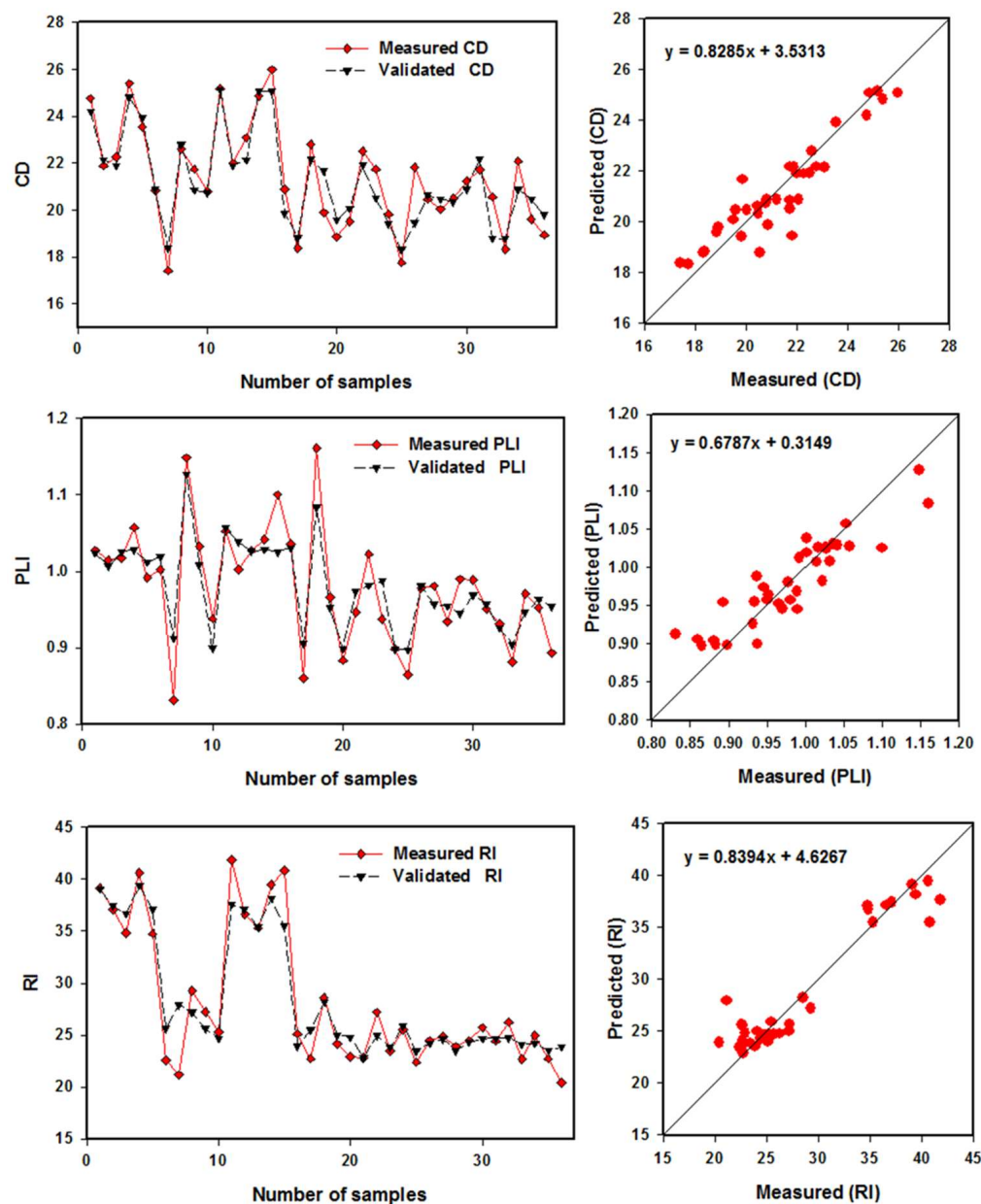


Figure 4. Comparison between measuring datasets, and validating datasets pollution load index (PLI), contamination (CD), and potential ecological risk index (RI) in two years using the RF models dependent on several elements.

The best suggested components (PCs) based on the outputs were the premium integration to filter the topmost variables, as detailed in Table 12. These elements were provided a high priority for assessing the sediment’s considered properties. The neural network was trained using the super elements’ attributes for predicting the researched parameters. Based on determination coefficient (R^2) values (Table 12) and slope (Figure 6), the BPNN model produced a more accurate evaluation of CD, PLI, and RI in both models of the Cal. and Val. The ANN-PCs-CD-17 model performed the best and demonstrated a better association between exceptional qualities and CD. The seventeen characteristics included in this model are critical for predicting CD with R^2 , values of 1.00 for (Cal.) and 1.00 for (Val.). The ANN-PCs-PLI-17 model performed the best in terms of measuring PLI with R^2

values for the Cal. and Val. of 1.00 and 0.98, respectively. The ANN-PCs-RI-17 model was the most accurate in detecting RI ($R^2 = 1.00$ for both Cal. and Val. datasets). The following considerations optimized the learning curve of the ANN model in this study: number and attributes of nominated features, selecting the most important parameters, and defining iterations for neural networks to avoid model over-fitting. The model’s hyperparameter optimization is a crucial aspect that influences the accuracy of water content prediction. Hyperparameter selection has a significant impact on the performance of any ML model, and it has various advantages: It has the potential to increase the performance of ML algorithms [98] and enhance scientific studies’ repeatability and fairness [99]. Furthermore, because it has direct control over the behaviors of training algorithms, it can perform a significant role in refining the prediction model [100]. As Elsherbiny et al. [101] revealed, the performance of the ANN algorithm for robust prediction was improved by following some steps during training, including filtering super-features and tuning model hyperparameters. These results are consistent with the proposed ANN model that used all sensitive features to monitor environmental pollution indicators that significantly increase the model’s performance. As for [102], the findings demonstrated ANN’s enormous potential for simulating water quality factors. The training and test data had simulation accuracy of 0.8 to 0.9, as determined by the Nash–Sutcliffe coefficient of efficiency. As a result, a trained ANN model might possibly provide simulated values for desirable regions when measured data are absent but water quality models are required. Ubah et al. [103] showed that the ANN model can be a promising tool as the actual water quality data are very well-analyzed with good prediction. The training model performance evaluation shows that the R^2 values ranges from 0.981 to 0.990, 0.981 to 0.988, 0.981 to 0.989, and 0.981 to 0.989, for pH, TDS, EC, and Na, respectively. The testing model performance shows that the R^2 value ranges from 0.952 to 0.967, 0.953 to 0.970, 0.951 to 0.967, and 0.953 to 0.968, for pH, TDS, EC, and Na, respectively. This indicates a good model for predicting water quality parameters using ANN for irrigation purposes.

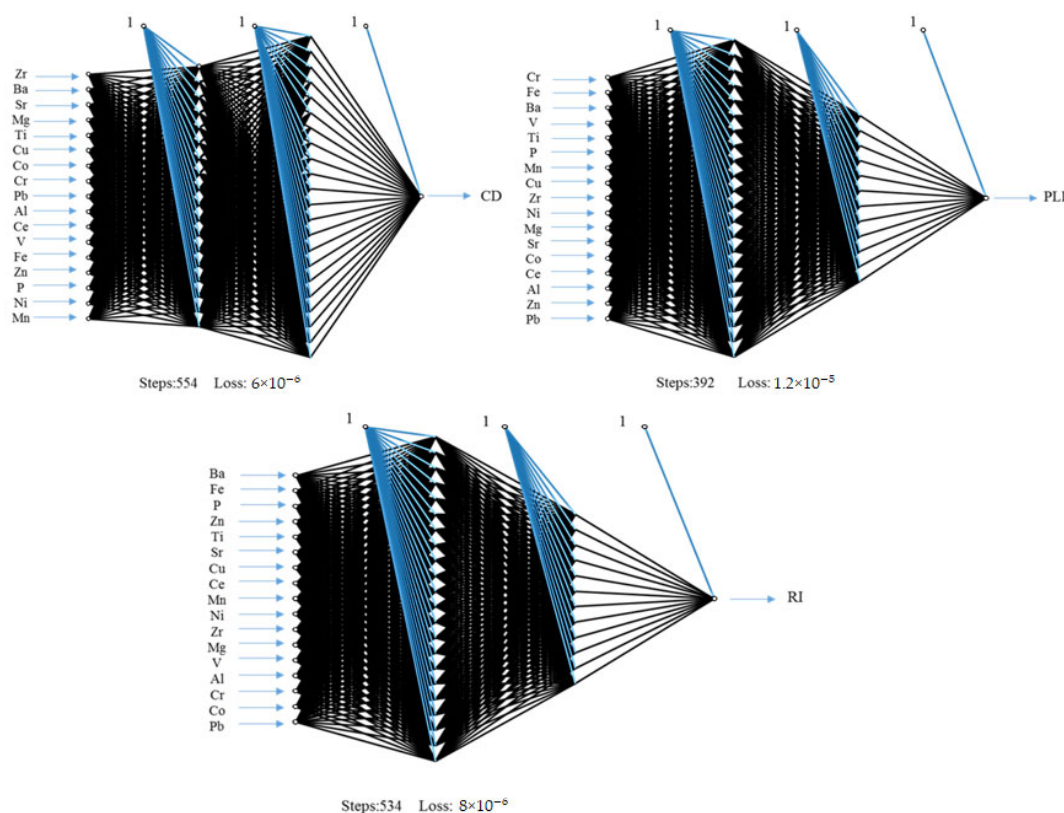


Figure 5. A neural network diagrams established for detecting contamination (CD), pollution load index (PLI), and potential ecological risk index (R1).

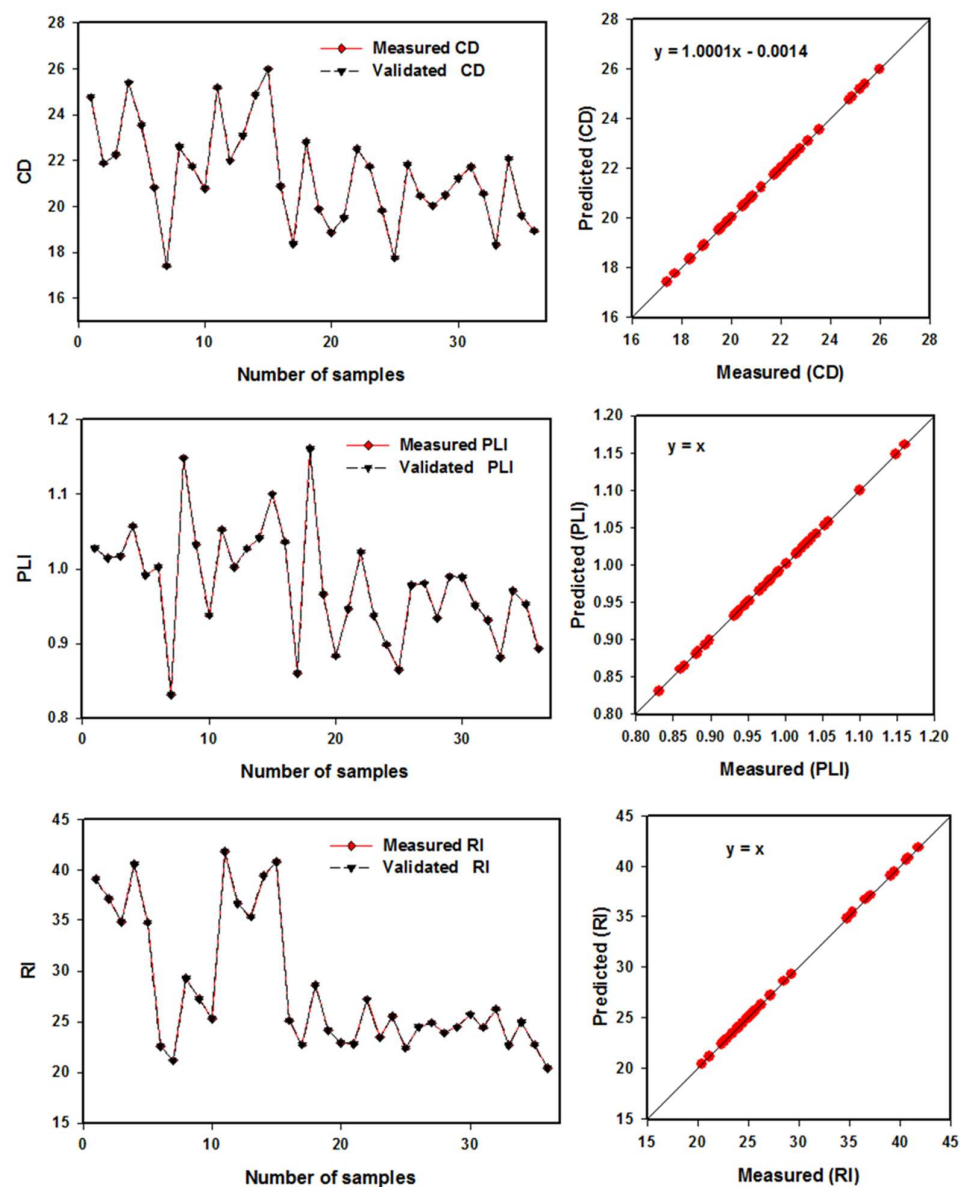


Figure 6. Comparison between measuring datasets, and validating datasets contamination (CD), pollution load index (PLI), and potential ecological risk index (RI) in two years using the ANN models. Statistical analysis was showed in Table 12.

4. Conclusions

The results of this study can be considered geo-environmental monitoring information on the eastern side of the Nile Delta Mediterranean coastal area. Several types of indices (single element indices such as CF, EF, and I_{geo} , and multi-element indices such as PLI, Dc, and RI) were employed to assess the rate of contamination and ecological risk of seventeen elements (Al, Mg, Cr, Cu, V, Sr, Ti, Zr, Ba, Ce, P, Mn, Fe, Ni, Pb, Co, and Zn) in surface sediments of the Gamasa estuary and coastal shelf. The RF and BPNN models were utilized to quantify the Dc, PLI, and RI. Al, Fe, and Mg concentrations were higher in sediment samples from the estuary and littoral shelf among the 17 tested elements. The estuary and littoral sediment samples were composed of a low concentration of Pb, Co, and Cu. The elevated concentrations of Al and Fe in the sediments indicated that terrigenous material had contaminated them. The CF results suggest that the Gamasa estuary and littoral shelf sediment samples are unpolluted by Al, Mg, Ni, Sr, Ba, and Ce, and highly polluted by Mn. The investigated sediment samples were considerably enriched by Cr, Co, Ni, Cu, Zr, V, Zn, P, and Mn and originated from anthropogenic sources. The enrichment shows that

anthropogenic sources, including sewage disposal, industrial and agricultural activity, as well as residential and urban wastes, contribute more to enrichment in the study area than natural sources. All the analyzed sediment samples were significantly contaminated by the tested elements according to the findings (Dc). According to the PLI findings, 70% of the Gamasa estuary samples is polluted, while 93.75 % of coastal shelf sediment is unpolluted. The potential ecological risk index revealed that the examined samples were classified as low ecological risk. The tested elements may be derived from natural sources, or they may be anthropogenic in origin and bind to clay minerals and hydroxides of iron. As a result, significant and essential actions must be taken to restrict sewage entry, treat sewage before it enters the estuary, and manage the water quality and sediments in the estuary. Elements in combination with RF and BPNN can be effective approaches for accurately estimating CD, PLI, and RI in Cal. and Val. datasets. For example, The RF-PCs-CD-17 model was better in predicting CD and was constructed using two (ntree: number of trees) and ten (ntree: number of trees). R^2 was increased to 0.85, using this model. The ANN-PCs-RI-17 model was the most accurate in detecting RI ($R^2 = 1.00$ for the Cal. and 1.00 for the Val.). In conclusion, the use of RF and BPNN techniques is recommended for assessing potentially toxic elements of surface sediment of aquatic environment.

Supplementary Materials: The following supporting information can be downloaded at: <https://www.mdpi.com/article/10.3390/jmse10060816/s1>, Table S1: Average concentrations of potential toxic elements in sediment samples collected from Gamasa estuary and littoral shelf (1st year); Table S2: Average concentrations of potential toxic elements in sediment samples collected from Gamasa estuary and littoral shelf (2nd year).

Author Contributions: Conceptualization, M.M.A.E.-S. and A.H.S.; methodology, M.M.A.E.-S., S.E., M.G. and A.H.S.; software, M.M.A.E.-S., S.E., O.E., M.G. and A.H.S.; validation, M.M.A.E.-S., S.E., O.E., A.H.E., M.G. and A.H.S.; formal analysis, M.M.A.E.-S., S.E., and A.H.S.; investigation, M.M.A.E.-S., S.E., O.E., M.G. and A.H.S.; resources, E.M.E., M.A.T., F.S.M., M.H.E.E.-M. and H.E.M.O.; data curation, M.M.A.E.-S., S.E., A.H.E., O.E., M.G. and A.H.S.; writing—original draft preparation, M.M.A.E.-S., S.E., and A.H.S.; writing—review and editing, M.M.A.E.-S., S.E., O.E., A.H.E., E.M.E. and A.H.S.; visualization, M.M.A.E.-S., S.E., O.E., F.S.M., M.G. and A.H.S.; supervision, A.H.S., S.E., E.M.E., M.A.T., M.H.E.E.-M. and H.E.M.O.; project administration, A.H.S., S.E., E.M.E., M.A.T., M.H.E.E.-M. and H.E.M.O.; funding acquisition, E.M.E., M.A.T., M.H.E.E.-M. and H.E.M.O. All authors have read and agreed to the published version of the manuscript.

Funding: This research was funded by King Khalid University (grant number RGP. 1/182/43), Abha, Saudi Arabia; The author (M.H.E. El-Morsy) would like to thank the Deanship of Scientific Research at Umm Al-Qura University for supporting this work by Grant Code: (22UQU4340486DSR01), Makkah, Saudi Arabia.

Data Availability Statement: Data are presented in the article and in Supplementary Materials.

Conflicts of Interest: The authors declare no conflict of interest.

References

1. Green, A.J.; Planchart, A. The neurological toxicity of heavy metals: A fish perspective. *Comp. Biochem. Physiol. C Toxicol. Pharmacol.* **2018**, *208*, 12–19. [[CrossRef](#)] [[PubMed](#)]
2. Sun, C.; Zhang, Z.; Cao, H.; Xu, M.; Xu, L. Concentrations, speciation, and ecological risk of heavy metals in the sediment of the Songhua River in an urban area with petrochemical industries. *Chemosphere* **2019**, *219*, 538–545. [[CrossRef](#)] [[PubMed](#)]
3. Zhang, H.; Walker, T.R.; Davisa, E.; Ma, G. Ecological risk assessment of metals in small craft harbour sediments in Nova Scotia, Canada. *Mar. Pollut. Bull.* **2019**, *146*, 466–475. [[CrossRef](#)] [[PubMed](#)]
4. Niu, Y.; Jiang, X.; Wang, K.; Xia, J.; Jiao, W.; Niu, Y.; Yu, H. Meta analysis of heavy metal pollution and sources in surface sediments of Lake Taihu, China. *Sci. Total Environ.* **2020**, *700*, 134509. [[CrossRef](#)] [[PubMed](#)]
5. Abou El-Safa, M.M.; Gad, M.; Eid, E.M.; Alnemari, A.M.; Almarshadi, M.H.; Alshammari, A.S.; Moghanm, F.S.; Saleh, A.H. Environmental Risk Assessment of Petroleum Activities in Surface Sediments, Suez Gulf, Egypt. *J. Mar. Sci. Eng.* **2021**, *9*, 473. [[CrossRef](#)]
6. Chen, H.; Wang, J.; Chen, J.; Lin, H.; Lin, C. Assessment of heavy metal contamination in the surface sediments: A reexamination into the offshore environment in China. *Mar. Pollut. Bull.* **2016**, *113*, 132–140. [[CrossRef](#)]

7. Guo, B.; Liu, Y.; Zhang, F.; Hou, J.; Zhang, H.; Li, C. Heavy metals in the surface sediments of lakes on the Tibetan Plateau, China. *Environ. Sci. Pollut. Res.* **2018**, *25*, 3695–3707. [[CrossRef](#)]
8. Pan, K.; Wang, W.X. Trace metal contamination in estuarine and coastal environments in China. *Sci. Total Environ.* **2012**, *421*, 3–16. [[CrossRef](#)]
9. Pang, H.J.; Lou, Z.H.; Jin, A.M.; Yan, K.K.; Jiang, Y.; Yang, X.H.; Chen, C.T.A.; Chen, X.G. Contamination, distribution, and sources of heavy metals in the sediments of Andong tidal flat, Hangzhou Bay, China. *Cont. Shelf Res.* **2015**, *110*, 72–84. [[CrossRef](#)]
10. Wardhani, E.; Rossmi, D.; Notodarmojo, S. Status of heavy metal in sediment of Saguling Lake, West Java. *IOP Conf. Ser. Earth Environ. Sci.* **2017**, *60*, 012035. [[CrossRef](#)]
11. Szydłowski, K.; Rawicki, K.; Burczyk, P. The content of heavy metals in bottom sediments of the watercourse in agricultural catchment on the example of the river Gowienica. *Inżynieria Ekol.* **2017**, *18*, 218–224. [[CrossRef](#)]
12. Tytła, M.; Kostecki, M. Ecological risk assessment of metals and metalloids in bottom sediments of water reservoir located in the key anthropogenic “hot spot” area (Poland). *Environ. Earth Sci.* **2019**, *78*, 179. [[CrossRef](#)]
13. Masria, A.; Negm, A.; Iskander, M.; Saavedra, O. Coastal zone issues: A case study (Egypt). *Procedia Eng.* **2014**, *70*, 1102–1111. [[CrossRef](#)]
14. Zhang, M.; He, P.; Qiao, G.; Huang, J.; Yuan, X.; Li, Q. Heavy metal contamination assessment of surface sediments of the Subei Shoal, China: Spatial distribution, source apportionment and ecological risk. *Chemosphere* **2019**, *223*, 211–222. [[CrossRef](#)] [[PubMed](#)]
15. Vetrimerugan, E.; Shruti, V.C.; Jonathan, M.P.; Royd, P.D.; Sarkar, S.K.; Rawlins, B.K.; Villegas, L.E.C. Comprehensive study on metal contents and their ecological risks in beach sediments of KwaZulu-Natal province, South Africa. *Mar. Pollut. Bull.* **2019**, *149*, 110555. [[CrossRef](#)] [[PubMed](#)]
16. Okbah, M.A.; Nasr, S.M.; Soliman, N.F.; Khairy, M.A. Distribution and Contamination Status of Trace Metals in the Mediterranean Coastal Sediments, Egypt. *Soil Sediment Contam. Int. J.* **2014**, *23*, 656–676. [[CrossRef](#)]
17. Soliman, N.F.; Nasr, S.M.; Okbah, M.A. Potential ecological risk of heavy metals in sediments from the Mediterranean coast, Egypt. *J. Environ. Health Sci. Eng.* **2015**, *13*, 70. [[CrossRef](#)]
18. El-Gamal, A.A.; Saleh, I.H. Geochemical Assessment of Heavy Metals Pollution and Ecological Risk in the Nile Delta Coastal Sediments, Egypt. *J. King Abdulaziz Univ. Mar. Sci.* **2016**, *26*, 41–59. [[CrossRef](#)]
19. Abdallah, M.A.M.; Badr-ElDin, A.M. Ecological risk assessment of surficial sediment by heavy metals from a submerged archaeology harbor, South Mediterranean Sea, Egypt. *Acta Geochim.* **2020**, *39*, 226–235. [[CrossRef](#)]
20. Khaled, A.; Ahdy, H.H.H.; Hamed, E.A.E.; Ahmed, H.O.; Abdel Razek, F.A.; Abdel Razek, M.A.; Elmasry, E. Spatial distribution and potential risk assessment of heavy metals in sediment along Alexandria Coast, Mediterranean Sea, Egypt. *Egypt. J. Aquat. Res.* **2021**, *47*, 37–43. [[CrossRef](#)]
21. CAPMAS. The Central Agency for Public Mobilization and Statistics. The Arab Republic of Egypt. 2021. Available online: <http://www.capmas.gov.eg/> (accessed on 22 April 2022).
22. EEAA (Egyptian Environmental Affairs Agency). National Circumstances. *Egypt Second National Communication on Climate Change*. 2010. Available online: <https://unfccc.int/resource/docs/natc/egyenc2.pdf> (accessed on 22 April 2022).
23. El-Sharnouby, B.A.; El-Alfy, K.S.; Rageh, O.S.; El-Sharabasy, M.M. Coastal Changes along Gamasa Beach, Egypt. *J. Coast. Zone Manag.* **2015**, *18*, 393. [[CrossRef](#)]
24. Sarkar, A.; Pandey, P. River water quality modelling using artificial neural network technique. *Aquat. Procedia* **2015**, *4*, 1070–1077. [[CrossRef](#)]
25. Isiyaka, H.A.; Mustapha, A.; Juahir, H.; Phil-Eze, P. Water quality modelling using artificial neural network and multivariate statistical techniques. *Model Earth Syst. Environ.* **2019**, *5*, 583–593. [[CrossRef](#)]
26. Adnan, R.M.; Liang, Z.; El-Shafie, A.; Zounemat-Kermani, M.; Kisi, O. Daily streamflow prediction using optimally pruned extreme learning machine. *J. Hydrol.* **2019**, *577*, 123981. [[CrossRef](#)]
27. Saleh, A.H.; Elsayed, S.; Gad, M.; Elmetwalli, A.H.; Elsherbiny, O.; Hussein, H.; Moghanm, F.S.; Qazaq, A.S.; Eid, E.M.; El-Kholy, A.S.; et al. Utilization of Pollution Indices, Hyperspectral Reflectance Indices, and Data-Driven Multivariate Modelling to Assess the Bottom Sediment Quality of Lake Qaroun, Egypt. *Water* **2022**, *14*, 890. [[CrossRef](#)]
28. Šiljić Tomić, A.; Antanasijević, D.; Ristić, M.; Perić-Grujić, A.; Pocajt, V. Application of experimental design for the optimization of artificial neural network-based water quality model: A case study of dissolved oxygen prediction. *Environ. Sci. Pollut. Res. Int.* **2018**, *25*, 9360–9370. [[CrossRef](#)] [[PubMed](#)]
29. Saleh, A.H.; Gad, M.; Khalifa, M.M.; Elsayed, S.; Moghanm, F.S.; Ghoneim, A.M.; Danish, S.; Datta, R.; Moustapha, M.E.; Abou El-Safa, M.M. Environmental Pollution Indices and Multivariate Modeling Approaches for Assessing the Potentially Harmful Elements in Bottom Sediments of Qaroun Lake, Egypt. *J. Mar. Sci. Eng.* **2021**, *9*, 1443. [[CrossRef](#)]
30. Dorgham, M.; El-Tohamy, W.; Qin, J.; Abdel-Aziz, N.; El-Ghobashy, A. Mesozooplankton in a stressed area of the Nile Delta Coast, Egypt. *Egypt. J. Aquat. Biol. Fish.* **2019**, *23*, 89–105. [[CrossRef](#)]
31. El-Gamal, A.A.; Saleh, I.H. Radiological and mineralogical investigation of accretion and erosion coastal sediments in Nile Delta Region, Egypt. *J. Oceanogr. Mar. Sci.* **2012**, *3*, 41–55. [[CrossRef](#)]
32. US EPA (United States Environmental Protection Agency). *Methods for Collection, Storage and Manipulation of Sediments for Chemical and Toxicological Analyses: Technical Manual*; EPA-823-B-01-002; Office of Water: Washington, DC, USA, 2001.

33. 2000a. *E 1391-94*; Standard Guide for Collection, Storage, Characterization, and Manipulation of Sediments for Toxicological Testing. ASTM: Conshohocken, PA, USA, 2000; Volume 11.05, pp. 768–788.
34. US Environmental Protection Agency (EPA). *Method 3052: Microwave Assisted Acid Digestion of Siliceous and Organically Based Matrices*; Print Office: Washington, DC, USA, 1996; p. 20.
35. Håkanson, L. An ecological risk index for aquatic pollution control: A sedimentological approach. *Water Res.* **1980**, *14*, 975–1003. [[CrossRef](#)]
36. Guo, W.; Huo, S.; Xi, B.; Zhang, J.; Wub, F. Heavy metal contamination in sediments from typical lakes in the five geographic regions of China: Distribution, bioavailability, and risk. *Ecol. Eng.* **2015**, *81*, 243–255. [[CrossRef](#)]
37. Wang, A.; Wei, C.; Xu, Y.; Hakif, M.; Hassan, A.; Ye, X.; Hoe, K. Assessment of heavy metal pollution in surficial sediments from a tropical river-estuary-shelf system: A case study of Kelantan River, Malaysia. *Mar. Pollut. Bull.* **2017**, *125*, 492–500. [[CrossRef](#)] [[PubMed](#)]
38. Pekey, H. The distribution and sources of heavy metals in İzmit Bay surface sediments affected by a polluted stream. *Mar. Pollut. Bull.* **2006**, *52*, 1197–1208. [[CrossRef](#)] [[PubMed](#)]
39. Abraham, G.M.S.; Parker, R.J. Assessment of heavy metal enrichment factors and the degree of contamination in marine sediments from Tamaki Estuary, Auckland, New Zealand. *Environ. Monit. Assess.* **2008**, *136*, 227–238. [[CrossRef](#)] [[PubMed](#)]
40. Varol, M.; Canpolat, Ö.; Eriş, K.K.; Çağlar, M. Trace metals in core sediments from a deep lake in eastern Turkey: Vertical concentration profiles, eco-environmental risks and possible sources. *Ecotoxicol. Environ. Saf.* **2020**, *189*, 110060. [[CrossRef](#)]
41. Müller, G. Index of geoaccumulation in sediments of the Rhine River. *GeoJournal* **1969**, *2*, 108–118.
42. Tiwari, M.; Sahu, S.K.; Bhangare, R.C.; Ajmal, P.Y.; Pandit, G.G. Depth profile of major and trace elements in estuarine core sediment using the EDXRF technique. *Appl. Radiat. Isot.* **2013**, *80*, 78–83. [[CrossRef](#)]
43. Tomlinson, D.L.; Wilson, J.G.; Harris, C.R.; Jeffrey, D.W. Problems in the assessment of heavy-metal levels in estuaries and the formation of a pollution index. *Helgoländer Meeresunters.* **1980**, *33*, 566–575. [[CrossRef](#)]
44. Harikumar, P.S.; Nasir, U.P.; Rahman, M.P.M. Distribution of heavy metals in the core sediments of a tropical wetland system. *Int. J. Environ. Sci. Technol.* **2009**, *6*, 225–232. [[CrossRef](#)]
45. Maanan, M.; Saddik, M.; Maanan, M.; Chaibi, M. Environmental and ecological risk assessment of heavy metals in sediments of Nador lagoon, Morocco. *Ecol. Indic.* **2014**, *48*, 616–626. [[CrossRef](#)]
46. Wang, C.; He, S.; Zou, Y.; Liu, J.; Zhao, R.; Yin, X.; Zhang, H.; Li, Y.W. Quantitative evaluation of in-situ bioremediation of compound pollution of oil and heavy metal in sediments from the Bohai Sea, China. *Mar. Pollut. Bull.* **2019**, *150*, 110787. [[CrossRef](#)] [[PubMed](#)]
47. Cheng, W.H.; Yap, C.K. Potential human health risks from toxic metals via mangrove snail consumption and their ecological risk assessments in the habitat sediment from Peninsular Malaysia. *Chemosphere* **2015**, *135*, 156–165. [[CrossRef](#)] [[PubMed](#)]
48. Looi, L.J.; Aris, A.Z.; Yusoff, F.M.; Isa, N.M.; Haris, H. Application of enrichment factor, geoaccumulation index, and ecological risk index in assessing the elemental pollution status of surface sediments. *Environ. Geochem. Health* **2019**, *41*, 27–42. [[CrossRef](#)]
49. Zhuang, S.; Lu, X.; Yu, B.; Fan, X.; Yang, Y. Ascertaining the pollution, ecological risk and source of metal(loid)s in the upstream sediment of Danjiang River, China. *Ecol. Indic.* **2021**, *125*, 107502. [[CrossRef](#)]
50. Hanif, N.; Eqani, S.A.M.A.S.; Ali, S.M.; Cincinelli, A.; Ali, N.; Katsoyiannis, I.A.; Bokhari, H. Geo-accumulation and enrichment of trace metals in sediments and their associated risks in the Chenab River, Pakistan. *J. Geochem. Explor.* **2016**, *165*, 62–70. [[CrossRef](#)]
51. Jiang, D.; Wang, Y.; Zhou, S.; Long, Z.; Liao, Q.; Yang, J.; Fan, J. Multivariate analyses and human health assessments of heavy metals for surface water quality in the Xiangjiang River Basin, China. *Environ. Toxicol. Chem.* **2019**, *38*, 1645–1657. [[CrossRef](#)]
52. Baran, A.; Tarnawski, M.; Koniarz, T. Spatial distribution of trace elements and ecotoxicity of bottom sediments in Rybnik reservoir, Silesian–Poland. *Environ. Sci. Pollut. Res. Int.* **2016**, *23*, 17255–17268. [[CrossRef](#)]
53. Strobl, C.; Boulesteix, A.-L.; Kneib, T.; Augustin, T.; Zeileis, A. Conditional variable importance for random forests. *BMC Bioinform.* **2008**, *9*, 307. [[CrossRef](#)]
54. Breiman, L. Random forests. *Mach. Learn.* **2001**, *45*, 5–32. [[CrossRef](#)]
55. Schalkoff, J. *Artificial Neural Networks*; McGraw-Hill Companies Inc.: New York, NY, USA, 1997.
56. Haykin, S. *Neural Networks: A Comprehensive Foundation*, 2nd ed.; Prentice Hall: Hoboken, NJ, USA, 1999.
57. Li, J.; Yoder, R.; Odhiambo, L.O.; Zhang, J. Simulation of nitrate distribution under drip irrigation using artificial neural networks. *Irrig. Sci.* **2004**, *23*, 29–37. [[CrossRef](#)]
58. Byrd, R.H.; Lu, P.; Nocedal, J.; Zhu, C. A limited memory algorithm for bound constrained optimization. *Siam J. Sci. Comput.* **1995**, *16*, 1190–1208. [[CrossRef](#)]
59. Glorfeld, L.W. A methodology for simplification and interpretation of backpropagation-based neural network models. *Expert Syst. Appl.* **1996**, *10*, 37–54. [[CrossRef](#)]
60. Malone, B.P.; Styc, Q.; Minasny, B.; McBratney, A.B. Digital soil mapping of soil carbon at the farm scale: A spatial downscaling approach in consideration of measured and uncertain data. *Geoderma* **2017**, *290*, 91–99. [[CrossRef](#)]
61. Saggi, M.K.; Jain, S. Reference evapotranspiration estimation and modeling of the Punjab Northern India using deep learning. *Comput. Electron. Agric.* **2019**, *156*, 387–398. [[CrossRef](#)]
62. Wang, C.; Nie, S.; Xi, X.H.; Luo, S.Z.; Sun, X.F. Estimating the biomass of maize with hyperspectral and LiDAR data. *Remote Sens.* **2017**, *9*, 11. [[CrossRef](#)]

63. Zhu, J.; Huang, Z.H.; Sun, H.; Wang, G.X. Mapping forest ecosystem biomass density for Xiangjiang river basin by combining plot and remote sensing data and comparing spatial extrapolation methods. *Remote Sens.* **2017**, *9*, 241. [[CrossRef](#)]
64. El Baz, S.M.; Khalil, M.M. Assessment of trace metals contamination in the coastal sediments of the Egyptian Mediterranean coast. *J. Afr. Earth Sci.* **2018**, *143*, 195–200. [[CrossRef](#)]
65. Guen, C.; Tecchio, S.; Dauvin, J.; Roton, G.; Lobry, J.; Lepage, M.; Morin, J.; Lassalle, G.; Raoux, A.; Niquil, N. Assessing the ecological status of an estuarine ecosystem: Linking biodiversity and food-web indicators. *Estuar. Coast Shelf Sci.* **2019**, *228*, 106339. [[CrossRef](#)]
66. Guo, C.; Chen, Y.; Xia, W.; Qu, X.; Yuan, H.; Xie, S.; Lin, L. Eutrophication and heavy metal pollution patterns in the water suppling lakes of China's south-to-north water diversion project. *Sci. Total Environ.* **2020**, *711*, 134543. [[CrossRef](#)]
67. Bantan, R.; Al-Dubai, T.; Al-Zubieri, A. Geo-environmental assessment of heavy metals in the bottom sediments of the Southern Corniche of Jeddah, Saudi Arabia. *Mar. Pollut. Bull.* **2020**, *161*, 111721. [[CrossRef](#)] [[PubMed](#)]
68. Niu, L.; Li, J.; Luo, X.; Fu, T.; Chen, O.; Yang, O. Identification of heavy metal pollution in estuarine sediments under long-term reclamation: Ecological toxicity, sources and implications for estuary management. *Environ. Pollut.* **2021**, *290*, 118126. [[CrossRef](#)] [[PubMed](#)]
69. Bai, J.; Xiao, R.; Cui, B.; Zhang, K.; Wang, Q.; Liu, X.; Gao, H.; Huang, L. Assessment of heavy metal pollution in wetland soils from the young and old reclaimed regions in the Pearl River Estuary, South China. *Environ. Pollut.* **2011**, *159*, 817–824. [[CrossRef](#)]
70. Casado-Martínez, M.C.; Forja, J.M.; DelValls, T.A. A multivariate assessment of sediment contamination in dredged materials from Spanish ports. *J. Hazard. Mater.* **2009**, *163*, 1353–1359. [[CrossRef](#)] [[PubMed](#)]
71. Paches, M.; Martínez-Guijarro, R.; Aguado, D.; Ferrer, J. Assessment of the impact of heavy metals in sediments along the Spanish Mediterranean coastline: Pollution indices. *Environ. Sci. Pollut. Res.* **2019**, *26*, 10887–10901. [[CrossRef](#)] [[PubMed](#)]
72. El Nemr, A.M.; El Sikaily, A.; Khaled, A. Total and leachable heavy metals in muddy and sandy sediments of Egyptian coast along Mediterranean Sea. *Environ. Monit. Assess.* **2007**, *129*, 151–168. [[CrossRef](#)] [[PubMed](#)]
73. Abdel Ghani, S.; El Zokm, G.; Shobier, A.; Othman, T.; Shreadah, M. Metal pollution in surface sediments of Abu-Qir Bay and Eastern Harbour of Alexandria, Egypt. *Egypt. J. Aquat. Res.* **2013**, *39*, 1–12. [[CrossRef](#)]
74. El-Sorogy, A.S.; Tawfik, M.; Almadani, S.A.; Attiah, A. Assessment of toxic metals in coastal sediments of the Rosetta area, Mediterranean Sea, Egypt. *Environ. Earth Sci.* **2016**, *75*, 398. [[CrossRef](#)]
75. Amor, R.B.; Yahyaoui, A.; Abidi, M.; Chouba, L.; Gueddari, M. Bioavailability and Assessment of Metal Contamination in Surface Sediments of Rades-Hamam Lif Coast, around Meliane River (Gulf of Tunis, Tunisia, Mediterranean Sea). *J. Chem.* **2019**, *11*, 4284987. [[CrossRef](#)]
76. Chifflet, S.; Tedetti, M.; Zouch, H.; Fourati, R.; Zaghden, H.; Elleuch, B.; Quéméneur, M.; Karray, F.; Sayadi, S. Dynamics of trace metals in a shallow coastal ecosystem: Insights from the Gulf of Gabès (southern Mediterranean Sea). *AIMS Environ. Sci.* **2019**, *6*, 277–297. [[CrossRef](#)]
77. Omar, M.B.; Mendiguchía, C.; Er-Raioui, H.; Marhraoui, M.; Lafraoui, G.; Oulad-Abdellah, M.K.; García-Vargas, M.; Moreno, C. Distribution of heavy metals in marine sediments of Tetouan coast (North of Morocco): Natural and anthropogenic sources. *Environ. Earth Sci.* **2015**, *74*, 4171–4185. [[CrossRef](#)]
78. Diaz-de Alba, M.; Galindo-Riano, M.D.; Casanueva- Marenco, M.J.; Garcia-Vargas, M.; Kosore, C.M. Assessment of the metal pollution, potential toxicity and speciation of sediments from Algeciras Bay (South of Spain) using chemometric tools. *J. Hazard. Mater.* **2011**, *190*, 177–187. [[CrossRef](#)] [[PubMed](#)]
79. Nour, H.E.; El-Sorogy, A.S. Distribution and enrichment of heavy metals in Sabratha coastal sediments, Mediterranean Sea, Libya. *J. Afr. Earth Sci.* **2017**, *134*, 222–229. [[CrossRef](#)]
80. Merhaby, D.; Ouddane, B.; Net, S.; Halwani, J. Assessment of trace metals contamination in surficial sediments along Lebanese Coastal Zone. *Mar. Pollut. Bull.* **2018**, *133*, 881–890. [[CrossRef](#)] [[PubMed](#)]
81. Choi, K.Y.; Kim, S.H.; Hong, G.H.; Chon, H.T. Distributions of heavy metals in the sediments of South Korean harbors. *Environ. Geochem. Health* **2012**, *34*, 71–82. [[CrossRef](#)]
82. Diop, C.; Dewaelé, D.; Cazier, F.; Diouf, A.; Ouddane, B. Assessment of trace metals contamination level, bioavailability and toxicity in sediments from Dakar coast and Saint Louis estuary in Senegal, West Africa. *Chemosphere* **2015**, *138*, 980–987. [[CrossRef](#)] [[PubMed](#)]
83. Duodu, G.O.; Goonetilleke, A.; Ayoko, G.A. Comparison of pollution indices for the assessment of heavy metal in Brisbane River sediment. *Environ. Pollut.* **2016**, *219*, 1077–1091. [[CrossRef](#)]
84. Ahamad, M.I.; Song, J.; Sun, H.; Wang, X.; Mehmood, M.S.; Sajid, M.; Khan, A.J. Contamination level, ecological risk, and source identification of heavy metals in the hyporheic zone of the Weihe River, China. *Int. J. Environ. Res. Public Health* **2020**, *17*, 1070. [[CrossRef](#)]
85. Jaskuła, J.; Sojka, M.; Fiedler, M.; Wróżyński, R. Analysis of Spatial Variability of River Bottom Sediment Pollution with Heavy Metals and Assessment of Potential Ecological Hazard for the Warta River, Poland. *Minerals* **2021**, *11*, 327. [[CrossRef](#)]
86. Barik, S.K.; Muduli, P.R.; Mohanty, B.; Rath, P.; Samanta, S. Spatial distribution and potential biological risk of some metals in relation to granulometric content in core sediments from Chilika Lake, India. *Environ. Sci. Pollut. Res.* **2018**, *25*, 572–587. [[CrossRef](#)]
87. Vineethkumar, V.; Sayooj, V.V.; Shimod, K.P.; Prakash, V. Estimation of pollution indices and hazard evaluation from trace elements concentration in coastal sediments of Kerala, Southwest Coast of India. *Bull. Natl. Res. Cent.* **2020**, *44*, 198. [[CrossRef](#)]

88. Hronec, O.; Vilček, J.; Tomáš, J.; Adamiin, P.; Huttmanová, E. *Environmental Components Quality Problem Areas in Slovakia*; Mendelova Univerzita: Brno, Czech Republic, 2010; 227p.
89. Pavilonis, B.; Lioy, P.; Guazzetti, S.; Bostick, B.C.; Donna, F.; Peli, M.; Zimmerman, N.J.; Bertrand, P.; Lucas, E.; Smith, D.R.; et al. Manganese concentrations in soil and settled dust in an area with historic ferroalloy production. *J. Expo. Sci. Environ. Epidemiol.* **2015**, *25*, 443–450. [[CrossRef](#)] [[PubMed](#)]
90. Adimalla, N.; Qian, H.; Wang, H. Assessment of heavy metal (HM) contamination in agricultural soil lands in northern Telangana, India: An approach of spatial distribution and multivariate statistical analysis. *Environ. Monit. Assess.* **2019**, *191*, 246. [[CrossRef](#)] [[PubMed](#)]
91. Reimann, C.; Filzmoser, P.; Hron, K.; Kyňclová, P.; Garrett, R.G. A new method for correlation analysis of compositional (environmental) data—a worked example. *Sci. Total Environ.* **2017**, *607*, 965–971. [[CrossRef](#)]
92. Zhang, J.; Zhou, F.; Chen, C.; Sun, X.; Shi, Y.; Zhao, H.; Chen, F. Spatial distribution and correlation characteristics of heavy metals in the seawater, suspended particulate matter and sediments in Zhanjiang Bay, China. *PLoS ONE* **2018**, *13*, e0201414. [[CrossRef](#)] [[PubMed](#)]
93. Al-Wabel, M.I.; Sallam, A.E.-A.S.; Usman, A.R.A.; Ahmad, M.; El-Naggar, A.H.; El-Saeid, M.H.; Al-Faraj, A.; El-Enazi, K.; Al-Romian, F.A. Trace metal levels, sources, and ecological risk assessment in a densely agricultural area from Saudi Arabia. *Environ. Monit. Assess.* **2017**, *189*, 252. [[CrossRef](#)]
94. Nazneen, S.; Singh, S.; Raju, N.J. Heavy metal fractionation in core sediments and potential biological risk assessment from Chilika lagoon, Odisha state, India. *Quat. Int.* **2019**, *507*, 370–388. [[CrossRef](#)]
95. Elsayed, S.; Ibrahim, H.; Hussein, H.; Elsherbiny, O.; Elmetwalli, A.H.; Moghanm, F.S.; Ghoneim, A.M.; Danish, S.; Datta, R.; Gad, M. Assessment of water quality in Lake Qaroun using ground-based remote sensing data and artificial neural networks. *Water* **2021**, *13*, 3094. [[CrossRef](#)]
96. Elsherbiny, O.; Fan, Y.; Zhou, L.; Qiu, Z. Fusion of Feature Selection Methods and Regression Algorithms for Predicting the Canopy Water Content of Rice Based on Hyperspectral Data. *Agriculture* **2021**, *11*, 51. [[CrossRef](#)]
97. Thawornwong, S.; Enke, D. The adaptive selection of financial and economic variables for use with artificial neural networks. *Neurocomputing* **2004**, *56*, 205–232. [[CrossRef](#)]
98. Melis, G.; Dyer, C.; Blunsom, P. On the state of the art of evaluation in neural language models. *arXiv* **2017**, arXiv:1707.05589.
99. Bergstra, J.; Yamins, D.; Cox, D. Making a Science of Model Search: Hyperparameter Optimization in Hundreds of Dimensions for Vision Architectures. In Proceedings of the 30th International Conference on Machine Learning (ICML 2013), Atlanta, GA, USA, 16–21 June 2013; pp. 115–123.
100. Wu, J.; Chen, X.-Y.; Zhang, H.; Xiong, L.-D.; Lei, H.; Deng, S.-H. Hyperparameter optimization for machine learning models based on Bayesian optimization. *J. Electron. Sci. Technol.* **2019**, *17*, 26–40.
101. Elsherbiny, O.; Zhou, L.; Feng, L.; Qiu, Z. Integration of Visible and Thermal Imagery with an Artificial Neural Network Approach for Robust Forecasting of Canopy Water Content in Rice. *Remote Sens.* **2021**, *13*, 1785. [[CrossRef](#)]
102. Palani, S.; Liang, S.Y.; Tkalich, P. An ANN application for water quality forecasting. *Mar. Pollut. Bull.* **2008**, *56*, 1586–1597. [[CrossRef](#)] [[PubMed](#)]
103. Ubah, J.I.; Orakwe, L.C.; Ogbu, K.N.; Awu, J.I.; Ahaneku, I.E.; Chukwuma, E.C. Forecasting water quality parameters using artificial neural network for irrigation purposes. *Sci. Rep.* **2021**, *11*, 24438. [[CrossRef](#)]